Cell Biol Toxicol (2025) 41:59
https://doi.org/10.1007/s10565-025-09996-4

RESEARCH

Exosome-mediated effects of BRCA1 on cardiovascular artery disease

Hairui Yu · Dong Wei · Weiqian Liao · Xiaoming Shang · Dandan Li · Chunzhao Liu · Qimei Deng · Haiquan Huangfu

Received: 20 May 2024 / Accepted: 28 January 2025
© The Author(s) 2025

Abstract The progression of coronary artery disease atherosclerosis (CAD) is closely associated with cardiomyocyte apoptosis and inflammatory responses. This study focused on investigating the impact of BRCA1 in exosomes (Exo) derived from M1 macrophages on CAD. Through the analysis of single-cell RNA-seq datasets, significant communication between macrophages and cardiomyocytes in CAD patients was observed. BRCA1, identified as a significant apoptosis-related gene, was pinpointed through the assessment of differential gene expression and weighted gene co-expression network analysis (WGCNA). Experimental procedures involved BRCA1 lentivirus transfection of M1 macrophages, isolation of Exo for application to cardiomyocytes and smooth muscle cells, cell viability assessments, and characterization of Exo. The results showed that BRCA1-Exo from M1 macrophages induced cardiomyocyte apoptosis and affected smooth muscle cell behavior. In vivo studies further supported the exacerbating effects of BRCA1-Exo on CAD progression. Overall, the involvement of Exo carrying BRCA1 from M1 macrophages is evident in the induction of cardiomyocyte apoptosis and the regulation of smooth muscle cell behaviors, thereby contributing to CAD atherosclerosis progression. These findings unveil novel molecular targets that could have potential implications for CAD treatment strategies.

Keywords Coronary artery disease · Atherosclerosis · BRCA1 · Exosomes · Cardiomyocyte apoptosis · Smooth muscle proliferation

Highlights
- BRCA1 in Exosomes from M1 Macrophages Drives Atherosclerosis Development BRCA1-loaded exosomes released from M1 macrophages are shown to enhance atherosclerosis by promoting apoptosis and pathological changes in vascular cells.
- Exosomal BRCA1 Triggers Cardiomyocyte Pyroptosis Exosomes carrying BRCA1 induce pyroptosis in cardiomyocytes, contributing to coronary artery disease progression.
- BRCA1 Exosomes Enhance Vascular Smooth Muscle Cell Proliferation Exosomes derived from M1 macrophages stimulate the proliferation of vascular smooth muscle cells, aggravating atherosclerotic plaque formation.

Supplementary Information The online version contains supplementary material available at https://doi.org/10.1007/s10565-025-09996-4.

H. Yu · D. Wei · C. Liu · Q. Deng
Department of Preventive Medicine, Shenzhen Hospital of Shanghai University of Traditional Chinese Medicine, Shenzhen 518000, China

W. Liao · X. Shang · D. Li · H. Huangfu (✉)
Department of Cardiology, Shenzhen Hospital of Shanghai University of Traditional Chinese Medicine, Shenzhen 518000, China
e-mail: hfhq890902@126.com

Introduction

Coronary atherosclerotic heart disease (coronary artery disease, CAD) is caused by an imbalance

Published online: 13 March 2025

between coronary blood supply and myocardial demand due to functional or structural changes in the coronary arteries, also known as ischemic heart disease (Libby 2006; Fioranelli et al. 2018). CAD is one of the most common cardiovascular diseases globally, with a complex pathogenesis involving multiple cell types and molecular pathways (Duggan et al. 2022; Goldsborough et al. 2022; Medina-Leyte et al. 2021). Chemokines regulate signals related to both traditional and emerging risk factors for atherosclerosis. Once blood leukocytes, mainly monocytes/macrophages and T lymphocytes, enter the arterial intima, they establish communication with endothelial cells and smooth muscle cells (SMC), the resident cells within the arterial wall (Libby and Theroux 2005, Malakar et al. 2019). The Klotho/FGF23 axis is instrumental in the pathogenesis of CAD, which is a primary cause of mortality on a global scale. Research findings reveal the involvement of the Klotho/FGF23 axis in modulating myocardial apoptosis and the release of cytokines by activating the ERK/MAPK pathway, contributing to CAD progression (Jia et al. 2023). Single-cell genomics has revealed new cellular states during the phenotypic transition of SMC as potential therapeutic targets for atherosclerosis in both mice and humans (Pan et al. 2020). Furthermore, a significant proportion of CAD loci can regulate gene expression in vascular smooth muscle cells (VSMCs), affecting their behavior (Solomon et al. 2022). This study focuses on cardiomyocytes and SMC to explore the regulatory mechanisms of coronary atherosclerosis. These processes not only lead to myocardial dysfunction but also further promote the development of atherosclerosis (Del Buono et al. 2022; Jiang et al. 2021; Nakamura et al. 2022).

With deepening research, it is increasingly recognized that in-depth knowledge of the molecular pathways responsible for the pathophysiology of CAD is vital for the enhancement of more efficient treatments and preventative measures (Doenst et al. 2022; Räber et al. 2022; Dawson et al. 2022). Among the many molecules involved, communication between cells, particularly through Exo, has recently gained significant attention (Chang et al. 2021, Janakiraman et al. 2023). Recent advancements in omics technologies have enabled deeper insights into CAD pathogenesis, especially by integrating exosome and epigenetic analyses. For example, novel multi-omics platforms can elucidate CAD progression by identifying cellular and molecular mechanisms across cell types, aiding in the understanding of CAD heterogeneity and potential therapeutic targets (Benincasa et al. 2023). Integrating these approaches, particularly epigenomic and exosomal studies, could reveal complex intercellular interactions and regulatory mechanisms relevant to CAD treatment strategies. As key carriers of intercellular communication, Exo can transport a variety of biomolecules, including proteins, RNA, and DNA, mediating information exchange between cells and influencing cellular behavior and function (Kluszczynska and Czyz 2023; Thakur et al. 2022; Piperigkou et al. 2022). Understanding the specific role of Exo in CAD holds significant implications for identifying new therapeutic targets for the disease.

In cardiovascular diseases, macrophages play a complex role (Yap et al. 2023; Cai et al. 2023; Wei et al. 2023). Macrophages, an essential element of the immune system, have the capacity to transition into pro-inflammatory (M1) or anti-inflammatory (M2) states based on external stimuli (Li et al. 2021a, b; Yekhtin et al. 2022; Li et al. 2023). M1 macrophages are key in promoting inflammatory responses and accelerating atherosclerosis progression (Cheng et al. 2021; Wu et al. 2021a, b; Wu et al. 2021a, b). Atherosclerosis (AS) serves as the underlying pathology for numerous cardiovascular disorders, including myocardial infarction, stroke, and cardiovascular mortality. Macrophages are pivotal cellular mediators in the advancement of AS and participate in all phases of disease evolution. A crucial factor impacting atherosclerotic plaque formation and durability is the polarization of macrophages. M1 macrophages predominantly localize in unstable plaques or near the lipid core of advanced plaques, where they facilitate plaque infarction and rupture, in opposition to M2 macrophages, which demonstrate a converse pattern. Pro-inflammatory stimuli present in the plaque microenvironment induce M1 polarization, disrupting the balance between M1 and M2 macrophages (Chen et al. 2024). They not only participate directly in inflammatory responses but also influence the functions of other cells, including cardiomyocytes and VSMCs, through the secretion of Exo, thereby impacting CAD pathogenesis (Zhang et al. 2022). When contrasted with endothelial cells, SMCs may have more direct interactions with macrophages or Exo (Zhang et al. 2021; Zhai et al. 2022; Yan et al. 2020; Pan et al. 2020). The signaling molecules

carried by these Exo can regulate the behavior of target cells, such as promoting apoptosis, enhancing or inhibiting cell proliferation, and controlling cell migration and differentiation (Wu et al. 2022a, b; Melamed et al. 2023). Therefore, in-depth research into the role of macrophages and their Exo in CAD is vital in elucidating the molecular processes underlying the disease and pinpointing fresh therapeutic markers.

The BRCA1 gene and its protein are essential for maintaining genomic stability and controlling the cell cycle (Tutt et al. 2021; Crossley et al. 2022; Vázquez-García et al. 2022). While its role in DNA damage repair, particularly in homologous recombination (HR), is well-studied (Kong et al. 2022; Yuhas et al. 2021), recent research has begun to uncover its importance in cardiovascular health (Alsiary et al. 2018). BRCA1 influences cardiomyocyte survival and apoptosis, playing a role in heart disease pathogenesis (Lu et al. 2022; Incorvaia et al. 2024). Abnormal expression or mutations in BRCA1 may also be associated with atherosclerosis progression (Yalcinkaya et al. 2023; Lin et al. 2022). Thus, investigating BRCA1's role in cardiovascular diseases, especially its role in macrophage-cardiomyocyte communication, holds the potential for identifying new therapeutic targets.

Although BRCA1's role in biological processes has been extensively studied, its specific function in M1 macrophage-derived Exo, particularly in coronary artery atherosclerosis, remains unclear (Batulan et al. 2018). Understanding how macrophages influence cardiomyocyte apoptosis and CAD progression through Exo is still limited (Pal et al. 2021; Samstein et al. 2020; Mehta et al. 2020). Specifically, there is a gap in understanding how BRCA1 regulates target cell behavior through Exo. This knowledge gap limits our comprehensive understanding of CAD and hinders new therapeutic strategies.

The primary objective of this study is to investigate the function of BRCA1 in M1 macrophage-derived Exo and its impact on cardiomyocyte apoptosis and coronary artery atherosclerosis. Through a combination of single-cell RNA sequencing (scRNA-seq), transcriptomics, in vitro cell experiments, and animal models, this study seeks to uncover the mechanisms of BRCA1 in macrophage-cardiomyocyte communication and identify new therapeutic targets for CAD prevention and treatment. Our discoveries might offer fresh perspectives on the pathophysiology of CAD and contribute to developing novel therapies, particularly by modulating BRCA1 in macrophage-derived Exo to slow or reverse atherosclerosis. This research holds scientific significance and offers potential clinical strategies to enhance the quality of life and survival rates among individuals with CAD.

Materials and methods

scRNA-seq data download and processing

The dataset GSE234077, available through the Gene Expression Omnibus (GEO) platform (http://www.ncbi.nlm.nih.gov/geo/), provided single-cell transcriptomic profiles from carotid atheroma of patients undergoing carotid endarterectomy. Included in this dataset are samples GSM7445264, GSM7445269, and GSM7445271. Thorough analysis and integration of the data were performed employing R's "Seurat" package. The assurance of quality involved the identification of cells with $200 < \text{nFeature\_RNA} < 5000$ and $\text{percent.mt} < 20$, and the top 2000 highly variable genes were identified for further analysis (Hao et al. 2021). The scRNA-seq dataset underwent dimensionality reduction by utilizing principal component analysis (PCA) with a focus on the highly variable genes. The Elbowplot function within the Seurat package guided the selection of the first 20 principal components (PCs) for subsequent analysis. The FindClusters function was utilized to identify cell subgroups at the default resolution ($\text{res} = 1$), followed by nonlinear dimensionality reduction carried out by applying the t-SNE algorithm. Through the application of the Seurat package, marker genes were employed to distinguish between different cell subtypes, while the "SingleR" package was utilized for cell annotation (Ma et al. 2019a, b). Investigation into cell communication was accomplished by employing the "CellChat" package in R. Pseudo-time analysis was conducted with the "monocle" package, employing DDRTree for dimensionality reduction and establishing cellular trajectories grounded on the expression patterns of ordering genes (Butler et al. 2018; Trapnell et al. 2014).

High-throughput transcriptome sequencing data download and processing

The GEO database (http://www.ncbi.nlm.nih.gov/geo/) was the source for the GSE187701 dataset, which contains transcriptomic information about CAD macrophages. This dataset comprises the Control group (GSM5669322, GSM5669323, GSM5669324) and the Model group (GSM5669330, GSM5669331, GSM5669332). Through the "limma" package in R software, an analysis was performed to pinpoint the differentially expressed genes (DEGs). The criteria for selecting DEGs between the Control and Model groups were set to $|\log2FC| > 0$ and $P.adjust < 0.01$. The "pheatmap" package in R software facilitated the generation of a volcano plot to illustrate the DEGs (Ritchie et al. 2015).

Weighted gene co-expression network analysis (WGCNA)

Calculation of the median absolute deviation (MAD) was carried out first for each gene in the differential gene expression profile, leading to the exclusion of genes with the lowest 50% MAD values. Subsequently, the removal of outliers among genes and samples was conducted by employing the goodSamplesGenes function provided by the WGCNA R package. The creation of a scale-free co-expression network involved the application of WGCNA, setting the minimum module size to 40 and the soft-thresholding power to 3. Additionally, five co-expression modules were identified through the merging of modules with a distance lower than 0.4. The collection of genes in the grey module was deemed unclassifiable within other modules. The correlation between modules and groups was assessed using Pearson correlation tests ($P < 0.05$), identifying genes significantly associated with CAD within the most relevant module for further analysis (Pan et al. 2021).

Venn analysis

Upon searching for "pyroptosis" in the GeneCards database (https://www.genecards.org/), a gene set related to cell death was retrieved. Venn analysis was conducted to intersect the DEGs, the WGCNA gene set, and the "pyroptosis" gene set to identify key candidate genes.

Cell culture

Mouse cardiomyocyte-like cells HL-1 (BFN60804428), mouse carotid artery smooth muscle cells SMC (BFN60870116), and mouse macrophages Ana-1 (BFN608006336) were all purchased from BLUEFBIO. The HL-1 and SMC cells were maintained in high-glucose Dulbecco's Modified Eagle Medium (DMEM, 11965118, Gibco) with the addition of 10% FBS (10270106, Gibco) and 1% penicillin–streptomycin (15070063, Gibco) under the conditions of 5% CO_2 and 37 °C in a humidified incubator.

The maintenance of Ana-1 cells involved the use of RPMI 1640 medium (11,875,093, Gibco) enriched with 10% FBS (10,270,106, Gibco) and 1% penicillin–streptomycin (15,070,063, Gibco), under the same incubation conditions. Upon reaching approximately 80% confluency, cultures were passaged using 0.25% trypsin/EDTA (T4049, Sigma-Aldrich) (Silvestro et al. 2021). Macrophages Ana-1 were then stimulated with 50 ng/mL LPS (HY-D105, MCE) and 40 ng/mL IFN-γ (HY-P7071, MCE) for 24 h to induce an M1 phenotype (Yin et al. 2021). Co-culture setups involved M0 or M1 macrophages in the upper chamber and HL-1 cells in the lower chamber. Prior to co-culturing, M1 macrophages were treated with 10 μM GW4869 (HY-19363, MCE) for 8 h to inhibit the release of Exo (Wang et al. 2019). The experiment groups were designated as M0 + HL-1, M1 + HL-1, and M1 + HL-1 + GW4869.

For fluorescent labeling of HL-1 cells, CellTracker™ Deep Red Dye (C34565, Invitrogen) was used adhering to the instructions as recommended by the manufacturer. Concisely put, HL-1 cells numbering 1.5×10^5 were suspended in a medium devoid of serum and treated with a dye solution at 500 nM concentration. Post a 30-min incubation, the cells were cleansed with PBS, seeded onto 8-well chamber slides, and supplemented with PKH67-labeled Exo (at a ratio of 5×10^4 Exo per seeded cell) the following day. Representative images were captured using fluorescence microscopy 12 h after the addition of PKH67-Exo (Ragni et al. 2020).

Cell grouping and transfection

Lentiviral transfection was used to construct overexpression cell lines and corresponding control

cell lines, including BRCA1-overexpressing Ana-1 (oe-BRCA1) and its control cell line (oe-BRCA1). The siRNA sequences for knockdown were selected (Table 1), and siBRCA1 was directly introduced into Exo in vitro. The primary method used was electroporation to load exogenous siRNA into the Exo, which was then directly added to the cells for treatment (Muskan et al. 2024).

The process of lentivirus-mediated cell transfection included seeding 1×10^5 cells into 6-well plates. Transfection was carried out by introducing the medium containing the proper dosage of packaging lentivirus (MOI = 10, having a working titer of about 1×10^6 TU/mL) and 5 μg/mL polybrene (TR-1003, Sigma-Aldrich) to the cells upon reaching 70–90% confluency. An equivalent amount of medium was added to dilute polybrene following a 4-h transfection period. The medium refresh occurred at the 24-h interval post-transfection, and following this, 48 h post-transfection, cells underwent selection using 1 μg/mL puromycin (A1113803, Thermo Fisher) in order to secure stable transfectants (Zhi et al. 2021; Gao et al. 2022).

CCK-8 assay

Ell viability was measured using the CCK-8 assay kit (CK04, Dojindo Laboratories). Cells were seeded in 96-well plates at a density of 1×10^5 cells. Every 24 h, 10 μL of CCK-8 solution and 100 μL of serum-free medium were added to each well. After a 2-h incubation at 37 °C, optical density (OD) was measured at 450 nm. Cell survival rate % = [(Experimental well—Blank well) / (Control well—Blank well)] × 100% (Ma et al. 2019a, b).

Scratch healing assay

For the scratch healing assay, cells were cultured to full density (100%) in 6-well plates employing a serum-free medium. A scratch was created across the cell layer using a 200 μL pipette tip, followed by three times washes with PBS to remove detached cells. M1 macrophage-derived Exo was then added. Twenty-four hours post-scratch, the scratch width was observed under a microscope, photographed and recorded. The distance of the wound area was measured with 0 h as the control, and the relative migration rate was analyzed using ImageJ software (Chen et al. 2021).

Table 1 lentiviral transfection sequence

Name	Sequence (5'−3')
sh-NC	TTCTCCGAACGTGTCACGT
sh-BRCA1-1(Mouse)	CCTCACTTTAACTGACGCAAT
sh-BRCA1-2(Mouse)	GCTCAGTGTATGACTCAGTTT

ELISA assays

Levels of interleukins IL-18 (CSB-E04609m, CUSABIO), IL-1β (CSB-E08054m, CUSABIO), and IL-6 (ab222503, Abcam) in cell supernatants and peripheral blood were measured using ELISA kits. Antigens were diluted to optimal concentrations with coating buffer, added to an ELISA plate, and followed by the addition of enzyme-linked antibodies and substrate solution. The reaction was stopped with 50 μL of stop solution per well, and absorbance was measured at 450 nm using a Bio-Rad microplate reader (1,681,135, Bio-Rad, USA) within 20 min. Standard curves were plotted, and data were analyzed according to the manufacturer's instructions (Yun et al. 2021).

Exosome phagocytosis assay

Exo collected from the culture medium was labeled with PKH67 through the PKH67 Fluorescent Cell Linker Mini Kit (MINI67, Sigma-Aldrich) according to the manufacturer's instructions. After a 12-h co-cultivation with HL-1 cells, the labeled Exo was fixed in 4% paraformaldehyde and mounted with an antifade medium containing DAPI (4083, CST). Imaging and observation were conducted using a laser scanning confocal microscope (LSM 980, ZEISS). This experiment was repeated three times for consistency (Shu et al. 2022).

Exosome collection and characterization

Exo was isolated from Ana-1 macrophages using a Total Exosome Isolation Kit (4,478,359, Thermo Fisher). Briefly, Ana-1 cells were cultured in plates

until reaching 70% confluency. PBS was utilized for cell washing, followed by culturing the cells in DMEM with 10% FBS for a 24-h incubation. Collection of the cell culture medium was succeeded by sequential centrifugation steps: first at 500 × g for 10 min to get rid of cells, then at 10,000 × g for 20 min to eliminate cell debris, and finally at 100,000 × g for 2 h to pellet the Exo. Resuspension of the exosome pellet in PBS was conducted for the purpose of subsequent transmission electron microscopy (TEM) and nanoparticle tracking analysis (NTA) (Bu et al. 2021; Shu et al. 2022). For flow cytometry analysis, Exo was diluted 1:10,000 in PBS and stained for 30 min at 4 °C with antibodies against CD63-APC (143,905, Biolegend), CD81-APC (104,909, Biolegend), and GM130 Alexa Fluor® 488 (560,257, BD). After staining, samples were diluted to 1,000 µL with PBS for analysis by flow cytometry. A gating strategy was established by comparing PKH67-Exo with PBS + CFSE samples in the FITC channel to selectively identify stained Exo. The presence of PKH67-Exo positive cells was then assessed by flow cytometry (Ragni et al. 2020).

TEM and NTA

Exo (Exo) were fixed in 4% paraformaldehyde, dropped onto formvar-coated electron microscopy grids to air-dry, and stained with 12% phosphotungstic acid (P9761, Soleibao) for 5 min. Detailed observations and analyses of Exo morphology were then performed using a JEOL 1010 transmission electron microscope (JEOL) (Bu et al. 2021).

Prepared Exo samples were analyzed using the Nanosight LM10-HS system (Malvern Panalytical). For each Exo sample, 30-s videos were recorded to capture the movement trajectories of Exo particles in PBS, with the process repeated three times (Ragni et al. 2020).

Immunofluorescence staining

Cells were fixed in 4% paraformaldehyde (P0099, Beyotime) for 15 min, followed by three PBS washes. Mouse carotid artery and heart tissue sections, each 8 µm thick, were prepared and adhered to slides by fixing with 4% paraformaldehyde for 10 min, followed by three PBS washes. Permeabilization was achieved with 0.3% Triton X (BL935B, Biosharp), and blocking was performed with 1% bovine serum albumin (V900933, Sigma-Aldrich) and 10% goat serum (C0265, Beyotime) for 30 min. The cells or tissues were then incubated overnight at 4 °C with primary antibodies: BRCA1 (MA1-23,164, 1/100, ThermoFisher), CD86 (PA5-114,995, 1/100, ThermoFisher), CD80 (PA5-114,992, 1/100, ThermoFisher), Ki67 (MA5-14,520, 1/100, ThermoFisher), and αSMA (MA1-06110, 1/100, ThermoFisher). After three PBS washes, fluorescent secondary antibodies—goat anti-mouse IgG(H + L) Alexa Fluor® 488 (ab150113, 1/200, Abcam) and goat anti-rabbit IgG(H + L) Alexa Fluor® 647 (ab150083, 1/200, Abcam)—were applied and incubated for 2 h in the dark at room temperature. Following PBS washes, slides were mounted with an antifade medium containing DAPI (4083, CST). Apoptosis was assessed using the Image-iT LIVE Red and Green Caspase Detection Kit (I35106, Invitrogen), following the manufacturer's guidelines. Imaging was performed with a laser scanning confocal microscope (LSM 980, ZEISS). Each experimental group included tissue sections from five animals, with one section per animal and one field of view for imaging. The experiment was conducted three times, and positive cell density was quantified using ImageJ software (National Institutes of Health, USA) (Yang et al. 2022; Takeda et al. 2021).

RT-qPCR

The Trizol Reagent Kit (T9424, Sigma-Aldrich) was employed for extracting total RNA from various cell groups. Assessment of RNA quality and concentration was carried out with a UV–Vis spectrophotometer (ND-1000, Nanodrop, USA). mRNA levels were quantified following reverse transcription by applying the PrimeScript™ RT Reagent Kit (RR014B, TaKaRa, Japan). Performing quantitative real-time PCR (RT-qPCR) on the ABI 7500 PCR System (Applied Biosystems, USA) was accomplished using the TB Green® Premix Ex Taq™ Kit (RR420A, TaKaRa, Japan). The primer sequences for BRCA1 were: Forward: 5'-CGG AGAGCGCGGGAATTTTA-3', Reverse: 5'-GAG AAGCCCCAAGAGAGGTG-3'; and for GAPDH: Forward: 5'-AAGAGGGATGCTGCCCTTAC-3', Reverse: 5'-GTTCACACCGACCTTCACCA-3'. GAPDH functioned as the internal control in this

context. Utilizing the $2^{-\Delta\Delta Ct}$ technique, we computed the relative gene expression levels, where ΔΔCT quantifies the fold change in gene expression between the control and experimental groups; ΔCt was obtained by subtracting the Ct value of the target gene from that of the internal reference gene (Yang et al. 2023).

Western blot

The Protein Extraction Kit (BC3710, Solarbio, China) was utilized to extract total protein from cells or tissues, followed by centrifugation at 13,000 rpm for 15 min at 4 °C, and the protein concentration of the supernatant was quantified utilizing the BCA Protein Assay Kit (P0010, Beyotime, China). Separation of proteins was carried out utilizing SDS-PAGE, following which they were transferred onto PVDF membranes. Subsequent steps included blocking of the membranes with 5% non-fat milk for 1 h at room temperature and then incubation with diluted primary antibodies against BRCA1 (MA1-23,164, 1/1000, ThermoFisher), GSDMD (20,770–1-AP, 1/2000, Proteintech), Caspase-1 (ab138483, 1/1000, Abcam), Caspase-4 (ab25898, 1/1000, Abcam), and β-actin (#4967, 1/1000, CST). A secondary antibody, Anti-Rabbit IgG (7074, 1/1000, CST), was used for incubation following this step, lasting for 1 h at room temperature, and then the sample was washed thrice with TBST (3 × 5 min). After removing TBST, the application of ECL Prime Western Blotting Detection Reagent (WBULS0500, EMD Millipore, USA) led to the formation of membranes, which underwent a one-minute incubation period. Subsequently, any excess reagent was eliminated, and the membranes were sealed with plastic wrap. The membranes were then exposed to X-ray film in a dark box for 5–10 min for development and fixation. Image J software was utilized to quantify the band intensity, where β-actin was employed as the loading control (Wang et al. 2021a, b).

Flow cytometry analysis

The analysis of M1 and M2 macrophages in mouse peripheral blood from all experimental groups was conducted employing flow cytometry. Initially, collected blood samples were digested with 10 U/mL collagenase I (17,018,029, Gibco) and 30 U/mL DNase I (18,047,019, Invitrogen) in RPMI 1640 medium (11,875,119, Gibco) at 37 °C lasting 60 min. Subsequent filtration through a 40 μm nylon filter yielded a single-cell suspension. Post red blood cell lysis, cells were washed twice with complete RPMI 1640 medium and stained at 4 °C with specific antibodies: anti-CD80-APC (560,016), anti-CD86-PE (553,692), anti-CD206-PE (568,273), and anti-F4/80-PE (565,410), all purchased from BD Biosciences. Upon undergoing double PBS washes, the cells were sorted via a flow cytometer (Beckman Coulter, USA), and FlowJo software was utilized for the execution of data analysis (Liu et al. 2020a, b).

Additionally, the Vybrant FAM Caspase Assay Kit (V35118, Invitrogen) was used in conjunction with flow cytometry to detect cell apoptosis. Late apoptotic cells were identified in the upper right quadrant ($FLICA^{+}PI^{+}$), early apoptotic cells in the lower right quadrant ($FLICA^{+}PI^{-}$), necrotic cells in the upper left quadrant ($FLICA^{-}PI^{+}$), and viable cells in the lower left quadrant ($FLICA^{-}PI^{-}$). The experimental protocol was executed as per the guidelines specified by the manufacturer (Wang et al. 2021a, b).

The investigation into cell proliferation was performed by applying the Click-iT Plus EdU Kit (Thermo Fisher, Cat# C10418). Cells were first labeled with the dye provided in the kit and incubated with the labeled dye. The percentage of positive-labeled cells was then analyzed using flow cytometry.

Establishment of mouse models

Homozygous Apoe knockout mice lack the APOE protein, develop normally, but exhibit significantly elevated total plasma cholesterol levels and spontaneous atherosclerotic lesions. This model can be used to study the role of APOE in lipid metabolism, atherosclerosis, and neural injury, as well as to explore potential interventions that may alter the progression of atherosclerosis. The male mice utilized in this study were of the C57BL/6 J strain, aged 6–8 weeks, and weighing 23 ± 2 g, sourced from Jackson Laboratory. To investigate the mechanisms underlying CAD atherosclerosis, $ApoE^{-/-}$ male mice (C001507, C57BL/6 background) were procured from Cyagen. The mice were accommodated in SPF-grade animal

facilities that ensured humidity levels of 60%–65% and temperatures ranging from 22 °C to 25 °C, allowing them ad libitum access to food and water. Upon ensuring the mice's health status following a week of acclimatization, the experiments were initiated. Approval for the experimental procedures and animal use was granted by the Institutional Animal Ethics Committee.

Establishment of the atherosclerosis mouse model: ApoE$^{-/-}$ mice (8 weeks old) in each group were fed a high-fat diet (40% fat, 0.15% cholesterol, Western diet) (10,141, Sino Biological Inc.) for 12 weeks to induce the atherosclerosis model. The mice were injected with 200 μg Exo through the tail vein twice a week, starting two weeks prior to the conclusion of the experiment. The control group was administered the equivalent volume of PBS. Initial untreated tissues (NC in ApoE$^{-/-}$) were collected for subsequent experiments. After the final experiment, carotid artery and heart tissues from the ApoE$^{-/-}$ group (high-fat diet + PBS treatment), Exo.NC group (high-fat diet + Exo.NC treatment), and Exo.shBRCA1 group (high-fat diet + Exo.shBRCA1 treatment) were collected, with 6 mice per group. These tissues were stored at −80 °C for subsequent analysis (Qiao et al. 2021, Bu et al. 2021). The Exo.NC group comprises Exo derived from epithelial cells.

The carotid artery injury model was established as described in the literature (Liu et al. 2020a, b). Anesthesia was administered to C57BL/6 J mice in the Sham group (control group) and Surgery group via intraperitoneal injection of 50 mg/kg sodium pentobarbital (P3761, Sigma Aldrich), with 6 mice allocated to each group. The surgery was performed under a dissecting microscope, where a 0.38 mm diameter wire was inserted into the left common carotid artery and slid three times. The right common carotid artery served as an untreated control. After the procedure, the incision was sutured with surgical thread in the surgery group, while the Sham group received no treatment. Following a wire-induced injury to the carotid artery, 10 μg of Exo dissolved in PBS was perfused into the ligated segment of the injured carotid artery for 30 min. Then, 50 μg of Exo was loaded into a 50 μl solution of 20% polyethylene glycol F-127 (ST501, Beyotime) gel at 4 °C and applied locally to the external membrane surrounding the injured artery segment. After 28 days post-surgery, histological and immunohistochemical analyses were performed on both the left and right carotid arteries obtained from every group of mice (Wang et al. 2019).

Exosome biodistribution

To assess exosome biodistribution post-treatment in the in vivo animal model, Exo was labeled with DiI (Celltracker CM-DiI, Invitrogen) before administration (Liang et al. 2020). Simultaneously, 40 μm-thick frozen sections of the heart, liver, spleen, and lungs were counterstained with 4′,6-diamidino-2-phenylindole (DAPI) and analyzed for biodistribution via immunofluorescence staining 24 h later. To characterize the cell types containing administered Exo, DiI-labeled Exo was co-stained with VEGF (1:500, Millipore), GSDMD (ab219800, 1/100, Abcam), CD86 (#20,018, 1/100, CST), and αSMA (MA1-06110, 1/100, ThermoFisher), followed by goat anti-mouse and anti-rabbit Alexa Fluor 488 antibodies (1:750, Invitrogen). Images were acquired using a Leica TCS-SPE confocal microscope with maximum projection settings and a 40×objective. The number of double-positive cells was counted in at least 10 different fields using Image-Pro Plus 4.1 software (Otero-Ortega et al. 2017).

H&E staining

The collected neck arterial tissues were fixed in freshly prepared 4% neutral buffered formaldehyde for 24 h. The fixed tissues then underwent a series of gradient alcohol dehydration steps, clearing, and routine paraffin embedding. Using a microtome, continuous sections were cut at a thickness of 5 μm, followed by baking at 60 °C for 1 h and dewaxing in xylene. After hydration, H&E staining (C0105S, Beyotime) was performed. Sections were initially stained with hematoxylin for 3 min, briefly rinsed in distilled water for 10 s, and then differentiated in 1% hydrochloric acid ethanol for 10 s. After a 1-min rinse in distilled water, the sections were stained with eosin for 1 min. Following another 10-s rinse in distilled water, the sections were dehydrated through an alcohol gradient, cleared in xylene, and finally sealed with neutral resin (Park et al. 2022; Xie et al. 2020). The sealed slides were examined for pathological changes using an optical microscope (Olympus CK2).

Oil red O staining for observing mouse aortic lesions

After 12 weeks of HDF feeding, mice were euthanized. The collected aortas from each group were rinsed in cold phosphate-buffered saline to remove fat tissues and opened at the thoracic aorta and aortic arch. Rapid freezing in liquid nitrogen was used to preserve the aortic tissues after they were cleaned and embedded in the OCT compound. Tissues were sliced into 7 μm thick sections using a cryostat. These sections underwent staining with 0.5% Oil Red O solution at ambient temperature for 30 min, followed by a brief rinse in 70% ethanol to remove excess dye, and then washed with PBS. The utilization of an optical microscope (Olympus, Japan-manufactured, model CX43) facilitated the activities of observation and photography. Semi-quantitative evaluation of the results was conducted with the aid of Image Pro Plus software (Feng et al. 2023, Qiao et al. 2021).

Measurement of TG, TC, and LDL-C levels

After the final experiment, peripheral blood samples were retrieved from each group of mice. Triglyceride (TG) concentrations in serum were quantified utilizing a triglyceride assay kit (BC0625, Solarbio), serum total cholesterol (TC) levels were gauged employing a cholesterol assay kit (BC1985, Solarbio), and the measurement of serum low-density lipoprotein cholesterol (LDL-C) levels was carried out with an LDL-C assay kit (BC5335, Solarbio), all in accordance with the prescribed manufacturer's guidelines (Liang et al. 2021).

Immunohistochemical staining

Paraffin embedding was used to section the collected neck arterial and cardiac tissues. The sections were baked at 60 °C for 20 min, followed by two sequential immersions in xylene, each lasting 15 min. After dehydration in graded alcohol, the sections were further immersed in absolute alcohol for 5 min, then in 95%, 90%, 80%, and 70% alcohol for 10 min each. Endogenous peroxidase activity was inhibited on each slide by treating with 3% H_2O_2 at room temperature for 10 min. Antigen retrieval was performed by microwaving the slides in citrate buffer for 3 min, followed by a 10-min incubation at room temperature in the antigen retrieval solution, and three washes in PBS. Slides were then incubated in goat serum blocking solution (SL038, Solarbio) at room temperature for 20 min. Primary antibodies against GSDMD (ab219800, 1/100, Abcam), CD86 (#20,018, 1/100, CST), CD80 (PA5-114,992, 1/100, ThermoFisher), and αSMA (MA1-06110, 1/100, ThermoFisher) were applied and incubated overnight at 4 °C. After three washes with PBS, slides were incubated with secondary antibodies—goat anti-rabbit IgG (ab6721, 1:5000, Abcam) or goat anti-mouse IgG (ab205719, 1:5000, Abcam)—for 30 min. DAB chromogen solution (P0203, Beyotime) was used for color development, and staining was visualized under an optical microscope. Image capture followed staining completion. Each group included five animals, with one slide per animal and one field chosen for imaging. ImageJ software (NIH) was used to calculate the positive area percentage (Yang et al. 2023).

Statistical analysis

Our research was facilitated by the use of R version 4.2.1 together with the RStudio integrated development environment, with the RStudio version employed identified as 2022.12.0–353. Processing of the data was carried out utilizing GraphPad Prism 8.0, where the results were exhibited in the form of mean ± standard deviation (Mean ± SD). Two groups were compared through unpaired t-tests, while comparisons among multiple groups were conducted using one-way analysis of variance (ANOVA). The homogeneity of variances was examined through the application of Levene's test. In situations where variances demonstrated equality, pairwise comparisons were conducted utilizing Dunnett's T3 and LSD-t tests. Conversely, if variances were deemed unequal, the Dunnett's T3 test was performed. Intergroup comparisons were considered statistically significant at a level of $P < 0.05$ (Zhang et al. 2020).

Results

Single-Cell sequencing reveals key role of M1 macrophages in CAD atherosclerosis

To analyze key genes in CAD atherosclerosis, we downloaded scRNA-seq data associated with CAD atherosclerosis from the GEO database (GSM7445264, GSM7445269, GSM7445271) (Fig. 1A) and processed and integrated this data employing the Seurat package. Gene counts (nFeature_RNA), mRNA molecules (nCount_RNA), and the percentage of mitochondrial genes (percent.mt) were evaluated for all cells in the scRNA-seq data. The majority of cells exhibited nFeature_RNA < 5000, nCount_RNA < 20,000, and percent.mt < 20% (Figure S1A). The criteria of 200 < nFeature_RNA < 5000 and percent.mt < 25% were set

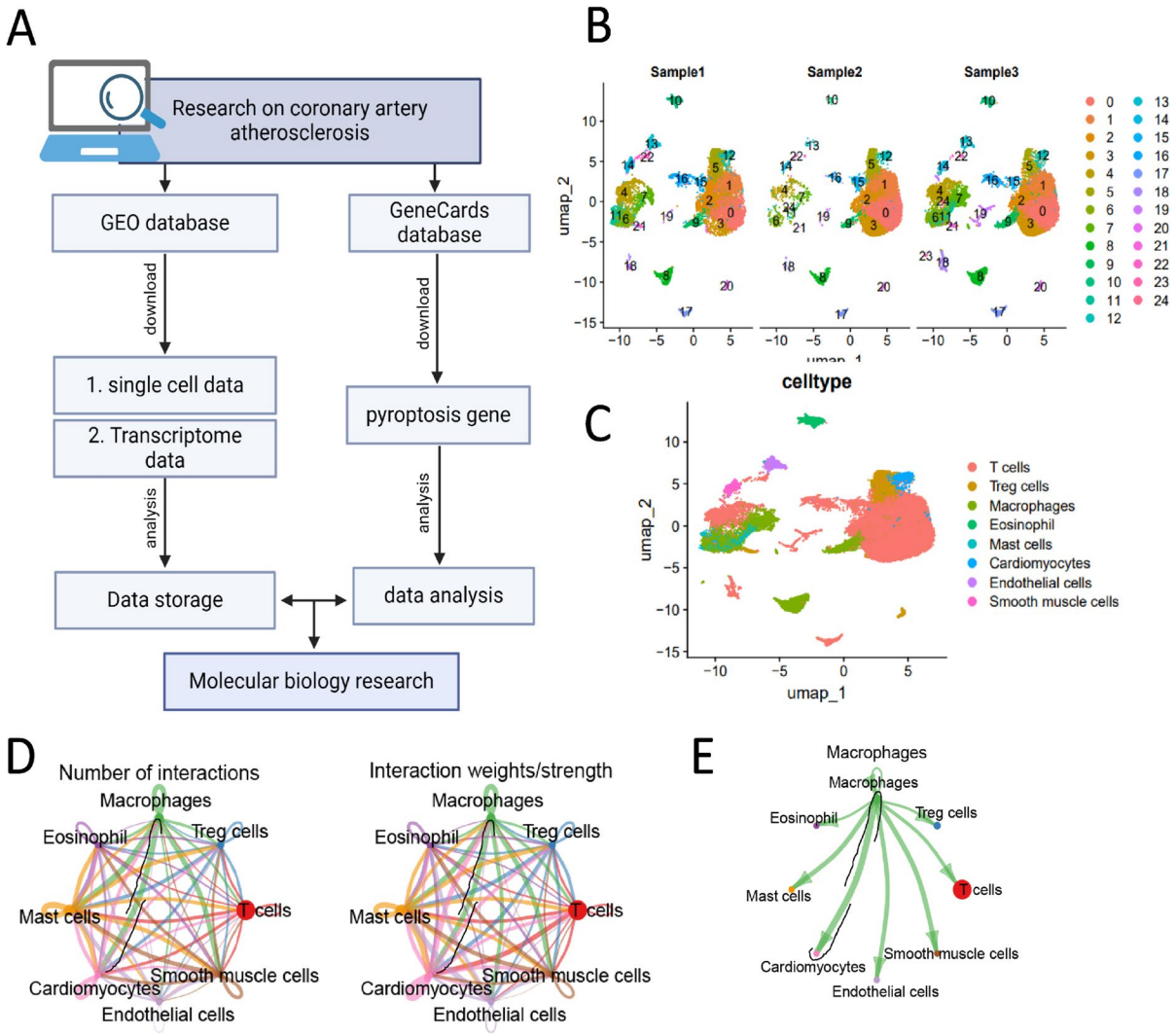

Fig. 1 Cell Clustering and Annotation from scRNA-seq Data. Note: (A) The foundational framework for studying cell heterogeneity and the progression of CAD atherosclerosis; (B) Analysis based on GSM7445264, GSM7445269, and GSM7445271 datasets downloaded from the GEO database, utilizing UMAP algorithm for dimensionality reduction and clustering visualization, showcasing cell populations isolated from carotid artery samples of CAD atherosclerosis patients, with each color representing a unique cell cluster; (C) Visualization of cell annotations based on UMAP clustering, where each color indicates a cell population; (D) Network analysis of cell communication based on the R package "CellChat"; (E) Analysis of macrophage communication networks with other cells using the R package "CellChat."

up for eliminating low-quality cells. As a result, an expression matrix comprising 16,153 genes and 18,253 cells was obtained.

Subsequently, we conducted sequencing depth correlation analysis, revealing a correlation coefficient of $r = -0.1$ between nCount_RNA and percent.mt, and $r = 0.87$ between nCount_RNA and nFeature_RNA (Figure S1B), indicating high data quality suitable for subsequent analyses.

Extended scrutiny of filtered cells included the identification of highly variable genes based on gene expression variance, whereby the top 2000 variable genes were singled out for further investigation (Figure S1C). Assessment of cell cycle scoring was accomplished through the use of the CellCycleScoring function, with data being preliminarily normalized. PCA was employed for linear dimensionality reduction (Figure S1D). We presented the main correlated gene expression heatmap for PC_1–PC_6 (Figure S1E) and the cell distribution in PC_1 and PC_2 (Figure S1F), indicating variations in batch effects among the samples.

Correcting data with the Harmony algorithm was carried out to tackle batch effects and enhance the precision of cell clustering (Figure S1G). Moreover, the ranking of PCs' standard deviations was accomplished through the ElbowPlot analysis, demonstrating that PC_1–PC_20 adequately encapsulated the data from genes with high variability and therefore possessed notable analytical significance (Figure S1H). Furthermore, we performed nonlinear dimensionality reduction using the UMAP algorithm on the top 20 PCs. UMAP clustering yielded 25 cell clusters (Fig. 1B), which were automatically annotated using the "SingleR" package, identifying 8 distinct cell types (Fig. 1C), including T cells, Treg cells, Macrophages, Eosinophils, Mast cells, Cardiomyocytes, Endothelial cells, and Smooth muscle cells.

Finally, to gain deeper insights into intercellular functional differences, the analysis of communication networks between distinct cell types was performed utilizing the "CellChat" package in R. Notably, in CAD atherosclerosis samples, we observed strong interactions between macrophages and cardiomyocytes (Fig. 1D-E), underscoring the potential significance of macrophages in the development of cardiovascular diseases associated with CAD atherosclerosis.

Integrated study reveals the prominent role of M1 macrophages in the advancement of CAD

To enhance the visual observation of dynamic changes in cellular states, we utilized a trajectory backbone graph based on Seurat clustering IDs to unveil the temporal ordering variations of individual cells in the pseudo-time analysis (Figure S2). This approach provides a more intuitive observation of dynamic cellular states and their potential transitions at different time points. For instance, it allows tracking of how cell populations transition gradually from one state to another, which is crucial for understanding cell fate determination and differentiation pathways. Leveraging scRNA-seq data, we performed pseudotime analysis using the R package monocle2. Visualization of ordering genes is depicted in Figure S2A, and data dimensionality reduction was achieved using DDRTree, providing a basis for subsequent cell ordering and trajectory construction (Figure S2B). The State-based display revealed cell evolution divided into 5 stages, including 2 critical branching nodes (Figure S2C).

Pseudotime, calculated by monocle2 based on cell gene expression information, represents the temporal sequence of cell development, where the root of the tree represents the starting point of time, and branches denote different cell fate paths. In the trajectory skeleton plot, the variation in color depth intuitively reflects cell ordering in pseudotime, revealing the developmental trajectory of cells from immature to mature states (Figure S2D). As shown in Fig. 2A, macrophages are in a relatively mature state, concentrating on the "origin" of differentiation. Pseudotime analysis further revealed the expression patterns of several key genes across different cell clusters. These gene expression levels exhibit significant differences among diverse cell types (e.g., T cells, macrophages), which is crucial for understanding the functional roles and state transitions of diverse cells in biological processes (Figure S2E). For instance, the expression patterns of C1QA, C1QB, and C1QC may be associated with cellular phagocytosis and immune responses, while ENO1 and RUNX3 expression may relate to cellular metabolic status and differentiation potential.

Additionally, pseudotime analysis revealed the differentiation patterns of the M1 macrophage markers CD86 and CD80, showing that CD86 and CD80 are specifically expressed in the early stages of cell

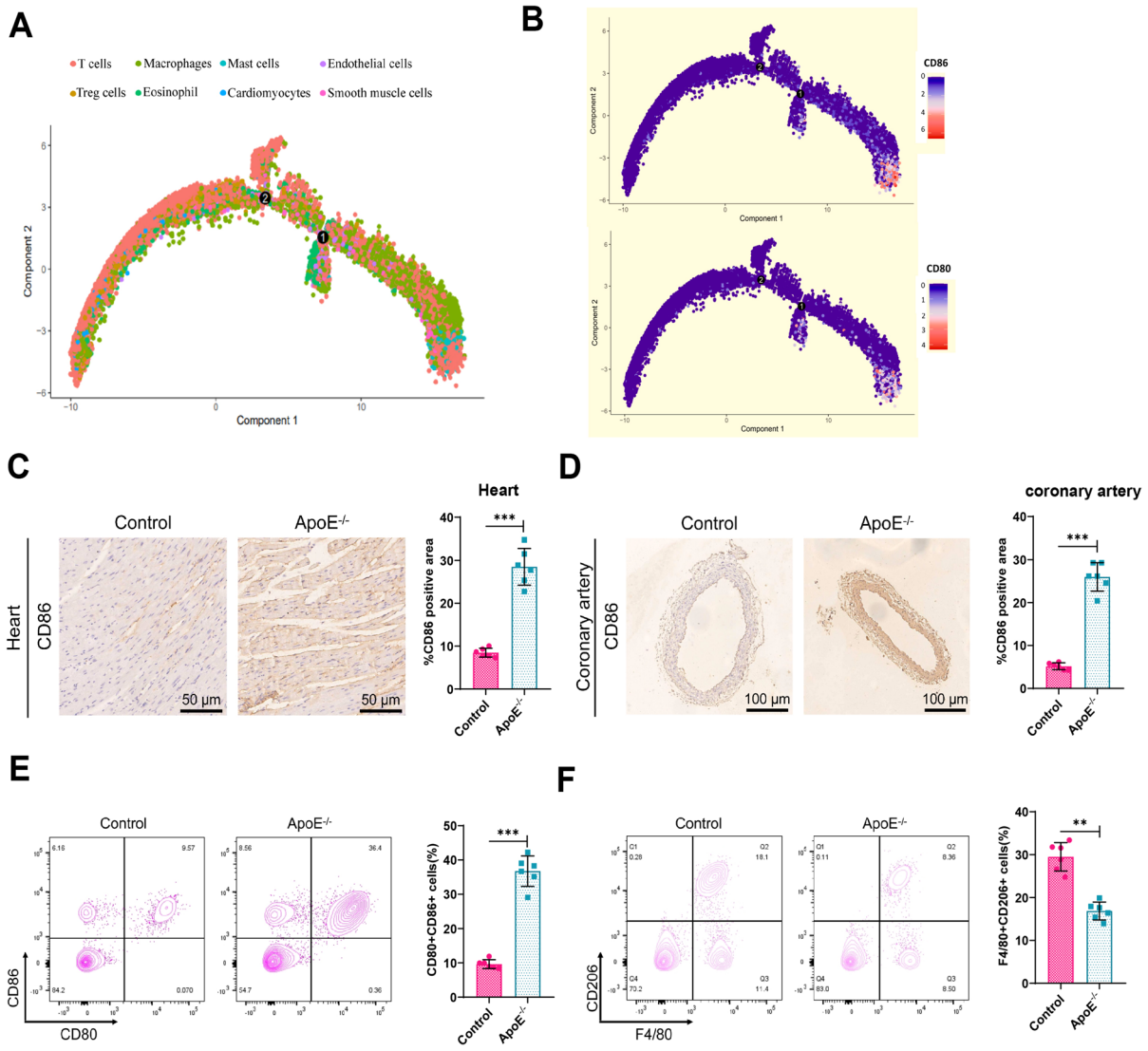

Fig. 2 The Close Association Between M1 Macrophages and the Progression of CAD. Note: (A) Trajectory skeleton map, mapping cells to pseudotime ordering based on Seurat's cluster ID; (B) Pseudotime analysis showing expression of M1 macrophage markers CD86 and CD80; (C) IHC analysis of CD86 expression in cardiac tissues of Control and ApoE$^{-/-}$ groups; (D) IHC analysis of CD86 expression in carotid tissues of Control and ApoE$^{-/-}$ groups; (E) Flow cytometry analysis of M1 macrophages (CD80^{+}CD86^{+}) in peripheral blood of Control and ApoE$^{-/-}$ groups; (F) Flow cytometry analysis of M2 macrophages (F4/80^{+}CD206^{+}) in peripheral blood of Control and ApoE$^{-/-}$ groups. ***$P<0.001$, **$P<0.01$, animal experiment n = 6

differentiation (Fig. 2B). This finding further confirms the close association between M1 macrophage activation and the progression of various inflammatory diseases, providing strong evidence for the dynamic changes of macrophage subgroups under different conditions. Furthermore, a mouse model of coronary artery atherosclerosis was induced in ApoE$^{-/-}$ mice through the administration of a high-fat diet for a duration of 12 weeks in vivo experiments. Sections were taken from the aortic arch of the mice's hearts, and Oil Red O staining revealed thickened intima with reddish-brown lipid plaque deposits. Additionally, in contrast with the Control group, the ApoE$^{-/-}$ group exhibited a notable augmentation in

the lesion area of the entire aorta and its root (Figure S3A-B). Moreover, the successful establishment of the model was evidenced by the elevated levels of TG, TC, and LDL-C in the $ApoE^{-/-}$ group's peripheral blood as opposed to the Control group (Figure S3C-E). Subsequently, immunohistochemical analysis verified the differential expression of CD86 in heart tissue and carotid artery tissue, revealing increased CD86 expression in the $ApoE^{-/-}$ group contrasted with the Control group in these tissue samples (Fig. 2C-D). Flow cytometry results also demonstrated an upregulation in the proportion of M1-type ($CD80^{+}CD86^{+}$) macrophages in the peripheral blood of the $ApoE^{-/-}$ group contrasted against the Control group, alongside a reduction in the presence of M2-type ($F4/80^{+}CD206^{+}$) macrophages (Fig. 2E-F), further confirming the close association between M1 macrophage activation and the development of CAD.

In summary, we have constructed a comprehensive view of cellular state changes that is mutually supportive and provides essential details for deciphering the function of macrophages in disease models.

Exo from M1 macrophages promote cardiomyocyte apoptosis

CAD, induced by coronary artery atherosclerosis, primarily manifests as cardiac blood supply insufficiency. This limitation hampers blood flow to the myocardium, resulting in myocardial ischemia and hypoxia, which may ultimately lead to cardiomyocyte damage or death (Dalen et al. 2014). During this process, cardiomyocyte apoptosis—a programmed cell death mechanism—significantly contributes to the pathological development of CAD (Sheng et al. 2023). M1 macrophages, integral to the immune system, secrete Exo containing various inflammatory factors and molecules that can enhance inflammatory reactions and potentially induce cardiomyocyte apoptosis (Tan et al. 2023). Given these findings, the crucial involvement of M1 macrophages in the initiation and progression of CAD atherosclerosis has been highlighted. Consequently, exploring how Exo produced by M1 macrophages affects cardiomyocytes, especially their role in cardiomyocyte apoptosis, is crucial for understanding the molecular mechanisms of myocardial inflammation and for developing potential therapeutic strategies.

Although HL-1 cardiomyocyte-like cells are a transformed cell line, they can still undergo continuous passaging while retaining the ability to contract and maintain the cardiac morphology, biochemical, and electrophysiological characteristics of differentiated cardiomyocytes. Therefore, they are suitable for the purposes of this study. The influence of macrophages on cardiomyocytes was examined by conducting an in vitro co-culture with HL-1 cardiomyocyte-like cells (Fig. 3A). Flow cytometry assessed the apoptosis ratio among HL-1 cells, revealing a significant increase in apoptosis in the M1 + HL-1 group compared to the M0 + HL-1 group (Fig. 3B). Synthesis of Exo occurs through the production of intraluminal vesicles within multivesicular bodies (MVBs), which are then released upon fusion of MVBs with the plasma membrane. Cargo sorting into intraluminal vesicles is facilitated by tetraspanin protein CD63, the Endosomal Sorting Complex Required for Transport complex, or by its affinity for ceramide-rich lipid microdomains dependent on neutral sphingomyelinase. Ceramide is a product formed when sphingomyelin (SM) is hydrolyzed by sphingomyelinase to remove phosphocholine. The addition of exogenous sphingomyelinase inhibitors or C6-ceramide can lead to the formation of vesicles (Arya et al. 2022).

GW4869, a non-competitive inhibitor of neutral sphingomyelinase C, employed to explore exosome production and secretion mechanisms (Habibi et al. 2022), was found to inhibit HL-1 cell apoptosis when added to the M1 + HL-1 group (Fig. 3B). Concurrently, immunofluorescence results showed a marked increase in apoptosis among HL-1 cells in the M1 + HL-1 group compared to the M0 + HL-1 group, an effect mitigated by GW4869, aligning with flow cytometry findings and suggesting that Exo from M1 macrophages promote cardiomyocyte apoptosis (Fig. 3C).

To delve further into the molecular basis of cell apoptosis under co-culture conditions, the quantification of GSDMD, Caspase-1, and Caspase-4 protein expression was carried out using Western blot analysis in diverse groups. When juxtaposed with the M0 + HL-1 group, the M1 + HL-1 group exhibited upregulated expression of these proteins, an effect suppressed by GW4869, thereby indicating a link between the apoptotic pathway and signaling through Exo from M1 macrophages (Fig. 3D).

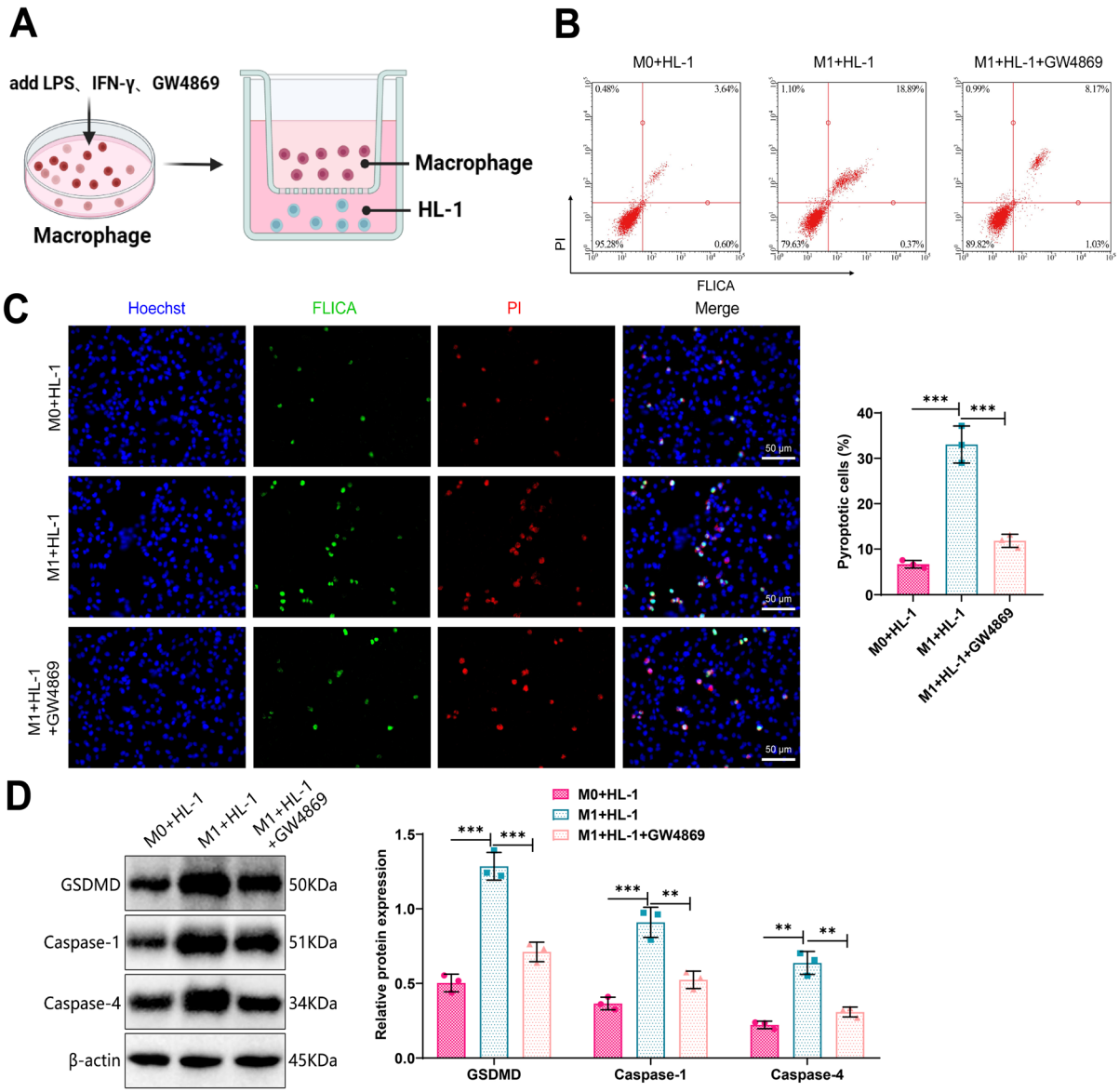

Fig. 3 Communication Analysis Between M1 Macrophages and Cardiomyocytes. Note: (A) Schematic of macrophage and HL-1 cell co-culture model; (B) Flow cytometry detection of HL-1 cell apoptosis post-co-culture, with $FLICA^{+}PI^{+}$ cells in quadrant Q2 representing apoptotic cells; (C) Immunofluorescence staining to detect apoptosis in HL-1 cells post-co-culture, with white arrows indicating apoptotic cells, Scale bar = 50 μm; (D) Western blot analysis of GSDMD, Caspase-1, and Caspase-4 expression in various cell groups post-co-culture. ***$P < 0.001$, cell experiment repeated 3 times

In conclusion, this segment of the study reveals that in a simulated inflammatory environment, the direct interaction between cardiomyocyte-like cells and macrophages, particularly through Exo produced by M1 macrophages, significantly accelerates cardiomyocyte-like cell apoptosis.

Transcriptome sequencing analysis identifies BRCA1 as a key molecule in promoting cardiomyocyte apoptosis

Building on previous findings that Exo from M1 macrophages facilitates cardiomyocyte apoptosis,

this study employed high-throughput transcriptome sequencing analysis to elucidate the molecular mechanisms by which macrophages promote cardiomyocyte apoptosis in CAD.

First, using the GEO database, we downloaded transcriptomic sequencing data related to CAD macrophages (GSM5669322, GSM5669323, GSM5669324, GSM5669330, GSM5669331, GSM5669332). Conducted differential expression analysis based on the criteria of |log2FC|>0 and $P<0.01$, leading to the discovery of 8,208 differentially expressed genes (DEGs), comprising 3,593 genes upregulated and 4,615 genes downregulated (Fig. 4A, Table S1). Subsequently, a gene co-expression network was built through the application of the WGCNA algorithm, with an appropriate threshold selected to enhance gene interconnectivity, ensuring the network adhered to scale-free network properties. The analysis determined an optimal threshold

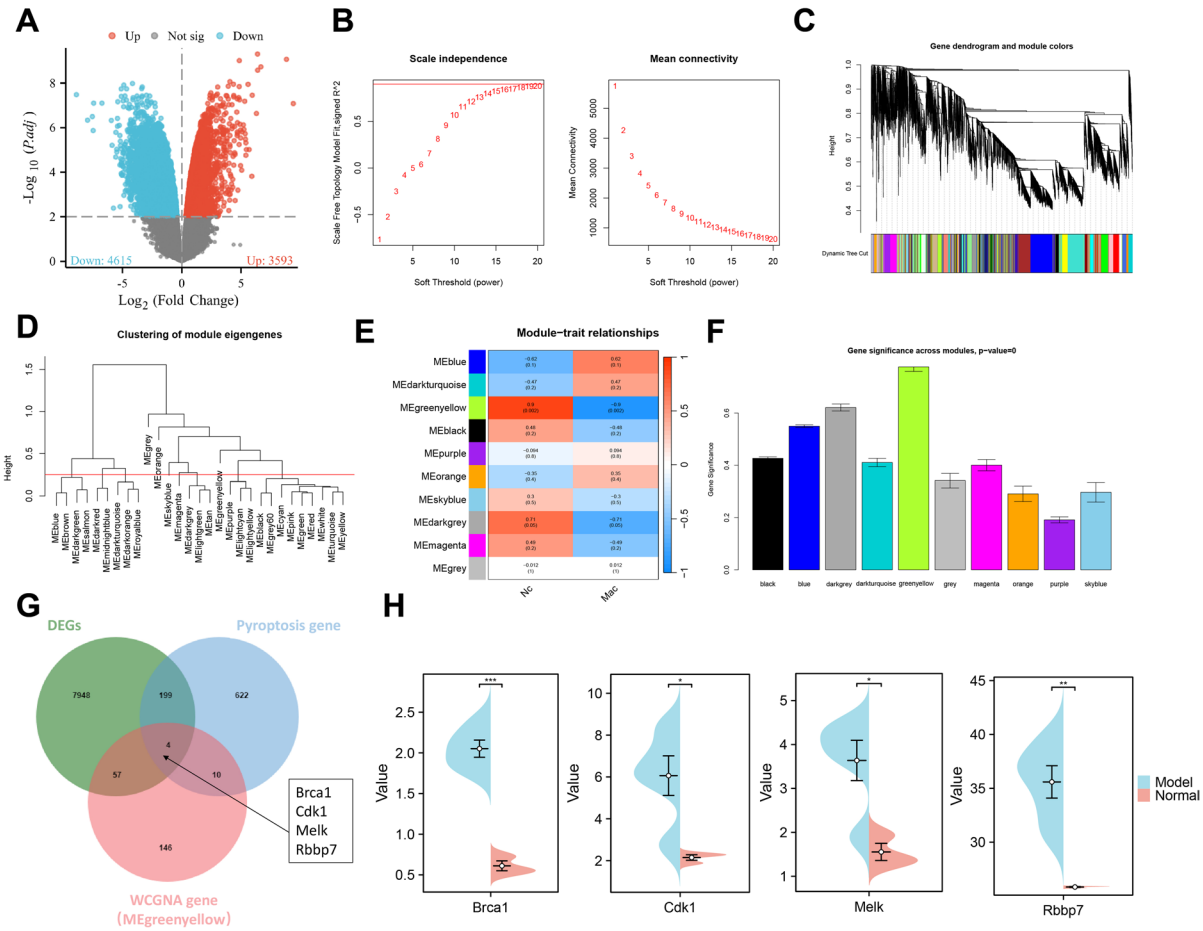

Fig. 4 Transcriptomic Analysis Combined with WGCNA Algorithm to Identify Key Genes Influencing CAD Progression. Note: (A) Volcano plot of differentially expressed genes from transcriptomic data of normal and model group heart macrophages based on GEO database analysis, including 3 normal and 3 model samples, with red indicating significantly upregulated genes, blue indicating significantly downregulated genes, and grey representing genes with no significant difference; (B) Scale independence, mean connectivity, and scale-free topology plot, determining the weighted value β = 19 to satisfy scale-free network laws; (C) Cluster dendrogram and trait heatmap of transcriptomic data from normal and model group mice samples; (D) Sample selection clustering dendrogram; (E–F) Heatmap (E) and bar graph (F) of gene module correlation with CAD and correlation analysis; (G) Intersection of "pyroptosis" related genes downloaded from GeneCards database with macrophage DEGs and WGCNA selected MEgreenyellow gene module in CAD progression; (H) Expression of intersected genes Brca1, Cdk1, Melk, Rbbp7 in heart macrophages of normal and model group mice. ***$P<0.001$, **$P<0.01$, *$P<0.05$

of 19, indicating a well-structured scale-free network (Fig. 4B). Using this threshold, genes within the CAD cohort were hierarchically clustered, and a dendrogram was constructed (Fig. 4C-D). Network modules were defined to contain at least 40 genes, and different gene modules were identified using dynamic tree cutting, with highly similar modules merged, resulting in ten distinct gene modules. The inter-module relationships were then analyzed (Fig. 4E-F), revealing that the MEgreenyellow module was significantly correlated with the progression of CAD, exhibiting the highest correlation. An intersection analysis of differentially expressed genes, CAD progression-related genes (MEgreenyellow module), and autophagy-related genes yielded four key genes (Fig. 4G): Brca1, Cdk1, Melk, and Rbbp7. Among these, Brca1 showed a marked upregulation in the Model group in relation to the Normal mice, marking the most notable difference ($P<0.001$) (Fig. 4H). Significance was also observed in alterations of Rbbp7, as depicted in Fig. 4H. Rbbp7, a nuclear protein expressed widely, falls under the category of WD repeat proteins that are highly conserved. It is present in complexes related to chromatin assembly. Furthermore, it has the capability to engage with the tumor suppressor gene BRCA1, suggesting its potential involvement in the modulation of cellular proliferation and differentiation (Yarden and Brody 1999; Yang et al. 2024; Chen et al. 2001). Given the low expression levels of Rbbp7 in normal macrophage tissues, Brca1 was chosen as the key molecule in this study. Through these comprehensive analyses, we not only uncovered critical transcriptomic changes in macrophages during CAD progression but also identified potential therapeutic targets for future treatment strategies.

Macrophage-Derived exo mediate cardiomyocyte apoptosis through BRCA1 delivery

Building upon preliminary research, this experiment posits that macrophages may promote cardiomyocyte apoptosis by transmitting the BRCA1 molecule. Consequently, this study aims to delve into the expression patterns of the BRCA1 gene within macrophages and their derived Exo and further analyze its potential impacts on cardiomyocytes. To achieve this objective, a series of experimental procedures were designed to investigate whether macrophage-derived Exo influences the biological characteristics of cardiomyocytes by delivering BRCA1.

Initially, analysis with NanoSight particle tracking revealed the size distribution of the Exo, which was found to be uniformly distributed within the nanometer size range of 100–130 nm, exhibiting typical characteristics of nanoscale vesicles (Fig. 5A). Subsequently, transmission electron microscopy provided visual evidence of the Exo morphology, displaying their typical spherical membrane structures (Fig. 5B). Furthermore, flow cytometry confirmed the identity of the Exo by detecting surface marker proteins CD81 and CD63 and the negative control protein GM130, establishing their high purity (Fig. 5C).

In quantifying the expression levels of BRCA1, this study utilized RT-qPCR and Western blot analyses. The results demonstrated a significant upregulation of BRCA1 mRNA levels in M1 macrophages compared to the M0 group (inactive macrophages), as well as in M1-Exo compared to M0-Exo, indicating an increase in BRCA1 mRNA levels within the Exo (Figure S4A). Western blot results aligned with RT-qPCR findings, further validating the elevation of BRCA1 protein levels in M1 macrophages and their derived Exo (Figure S4B).

To investigate the role of BRCA1 in intercellular communication, this experiment involved using M1 macrophages with either silenced or overexpressed BRCA1. The Exo released by these macrophages were collected and used to treat HL-1 cells (Fig. 5D). Evaluation through RT-qPCR was carried out to determine the efficiency of BRCA1 knockdown and overexpression in macrophages and the expression of BRCA1 mRNA in Exo (Figure S4C-D).

Exo, as a category of minuscule membrane-enclosed structures, facilitates communication between cells by carrying biomolecules, playing a significant role in immune responses and cell signaling (Rangel-Ramírez et al. 2022). Particularly, in the interactions between macrophages and other cell populations, Exo serves as a crucial mediator (Kishore and Petrek 2021). Immunofluorescence staining revealed CFSE-Exo positive particles in the cytoplasm of HL-1 cells (Fig. 5E), providing more direct evidence of potential physical contact between Exo and target cells.

Subsequent CCK-8 assays evaluated the impact of Exo derived from M1 macrophages on the viability of HL-1 cells. It was observed from the results that the cell viability was higher in the Exo.shBRCA1 group than in the Exo.NC (negative control) group; conversely, cell

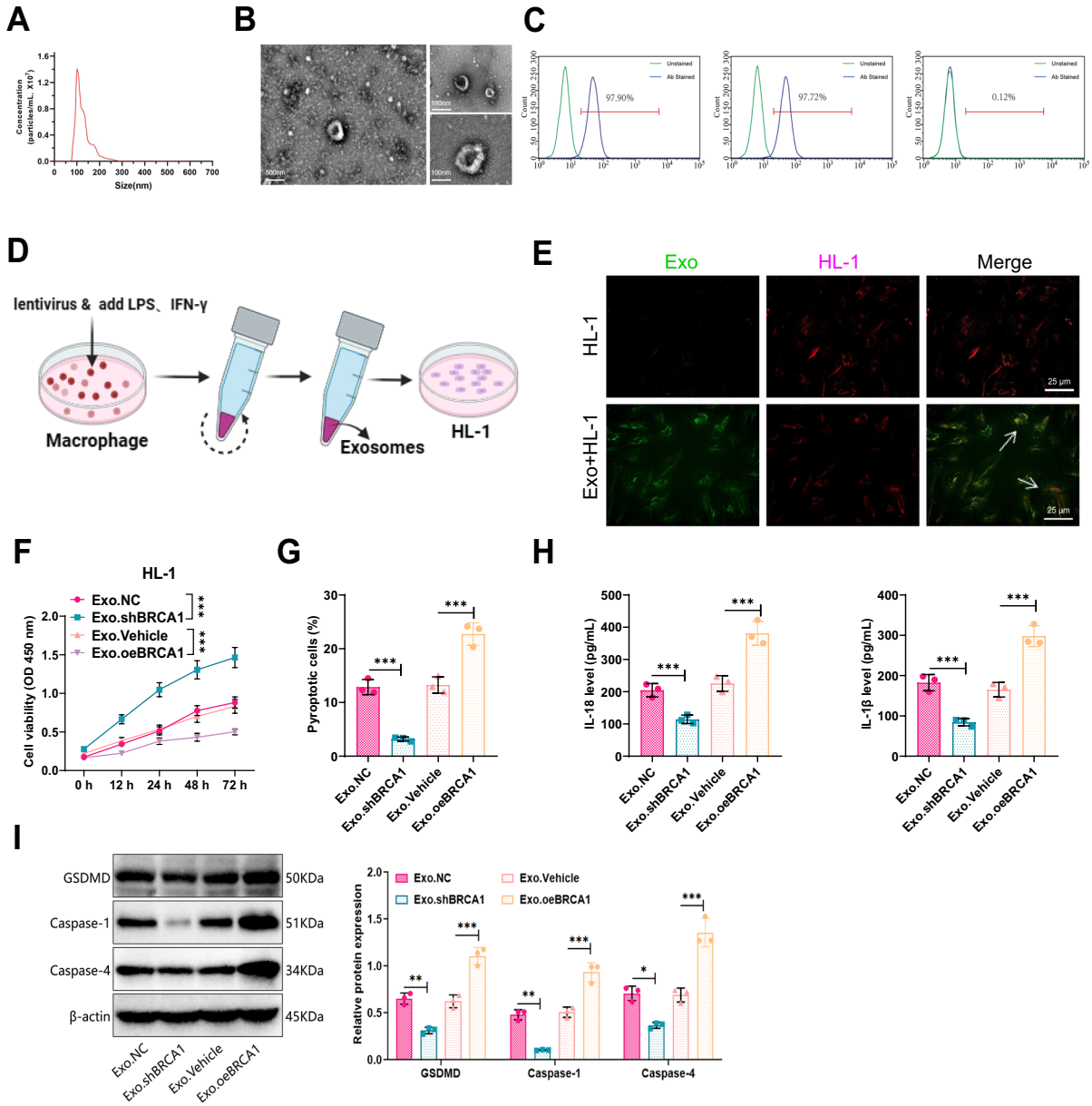

Fig. 5 Regulation of GSDMD and Caspase-1 Expression by BRCA1-Modified Exo. Note: (A) NanoSight particle tracking analysis of nanoscale particle size distribution in Exo derived from macrophages; (B) Transmission electron microscopy analysis of the nanoparticle morphology of Exo from macrophages, left image Scale bar = 500 nm, right image Scale bar = 100 nm; (C) Flow cytometry detection of exosomal markers (CD81 and CD63) expression, with GM130 serving as a negative control; (D) Schematic of HL-1 cells treated with Exo from M1 macrophages; (E) HL-1 cells stained with CellTracker™ Deep Red dye, immunofluorescence staining detecting the interaction between HL-1 cells and Exo, magenta represents HL-1 cells, green represents Exo, white arrows indicate the interaction in merged images, scale bar = 25 μm; (F) CCK8 assay to assess HL-1 cell viability; (G) Flow cytometry analysis of apoptosis in HL-1 cell groups; (H) ELISA measurement of inflammatory markers IL-18 and IL-1β in the supernatant of HL-1 cells treated with Exo; (I) Western blot analysis of GSDMD, Caspase-1, and Caspase-4 expression in HL-1 cells post-exosome treatment. $^{***}P < 0.001$, $^{**}P < 0.01$, $^{*}P < 0.05$, cell experiment repeated 3 times

viability decreased in the Exo.oeBRCA1 (overexpressing BRCA1) group relative to the Exo.Vehicle group, suggesting that the delivery of BRCA1 via Exo significantly affects HL-1 cell viability (Fig. 5F). Flow cytometry results further supported this hypothesis, showing a decrease in apoptosis rates in HL-1 cells in the Exo.shBRCA1 group in contrast with the Exo.NC group, and an increase in apoptosis rates in the Exo.oeBRCA1 group contrasted against the Exo.Vehicle group (Fig. 5G). Additionally, according to the ELISA results, the levels of IL-18 and IL-1β in the Exo.shBRCA1 group were markedly lower than those in the Exo.NC group, whereas they were substantially higher in the Exo.oeBRCA1 group when juxtaposed with the Exo.Vehicle group (Fig. 5H), reflecting the activation of inflammatory signaling pathways due to BRCA1 delivery. Western blot analysis further confirmed the expression levels of apoptosis-related proteins GSDMD, Caspase-1, and Caspase-4. When contrasted with the Exo.NC group, considerable drops in protein expression were observed in the Exo.shBRCA1 group, while noteworthy surges were noted in the Exo.oeBRCA1 group of HL-1 cells (Fig. 5I). A paradigm shift has occurred in the treatment of BRCA1/2-mutated human malignancies, as PARP1 is now recognized as a viable therapeutic target in BRCA1/2-deficient cells. However, studies have shown that PARP inhibitors induce inflammatory pyroptosis mediated by the caspase-3-dependent cleavage of GSDME (Kim et al. 2023). Additionally, research has demonstrated that BRCA1 protects VSMCs from oxidative stress (Lovren et al. 2014). Our experimental results (now shown in Fig. 5) also indicate changes in the aforementioned cytokines and proteins in the non-canonical pyroptosis pathway. Therefore, these experimental findings suggest that BRCA1 may influence cell viability and regulation through the non-canonical pyroptosis pathway, thereby promoting cardiomyocyte pyroptosis.

In summary, Exo derived from macrophages significantly promotes cardiomyocyte apoptosis by delivering the BRCA1 molecule.

Macrophage-Derived exo facilitate SMC cell proliferation and migration via *BRCA1 delivery*

This study delves into the impact of macrophage-derived Exo delivering BRCA1 protein on the functionality of VSMCs, particularly their role in vascular remodeling processes. CAD, especially the progression of atherosclerosis, involves complex vascular remodeling mechanisms following endothelial injury, where the migration, proliferation, and neointima formation by SMCs are central (Indolfi et al. 2019). Under healthy conditions, SMCs remain relatively quiescent within the vascular wall, maintaining vascular structure and function. However, in the atherosclerotic milieu, influenced by inflammatory cytokines, oxidative stress, and mechanical stress, SMCs transition from a contractile to a synthetic phenotype, characterized by enhanced migratory and proliferative capabilities, leading to intimal thickening and luminal narrowing, thereby exacerbating CAD progression (Meng et al. 2022).

First, using Exo with silenced or overexpressed BRCA1 to treat SMC cells, a scratch assay was executed to assess the migratory potential of SMC cells. The outcomes displayed that, in comparison with the Exo.NC group, the Exo.shBRCA1 group inhibited SMC cell migration, while contrasted against the Exo.Vehicle group, the Exo.oeBRCA1 group promoted SMC cell migration (Figure S5A). Additionally, the CCK8 assay results indicated that when juxtaposed with the Exo.NC group, the Exo.shBRCA1 group inhibited SMC cell viability, whereas contrasted against the Exo.Vehicle group, the Exo.oeBRCA1 group promoted SMC cell viability (Figure S5B). The Edu proliferation assay exhibited that relative to the Exo.NC group, the Exo.shBRCA1 group significantly inhibited SMC proliferation, with a drop in the number of positive cells, while the Exo.oeBRCA1 group increased the proportion of positive SMC cells contrasted with the Exo.Vehicle group (Figure S5C).

To delve deeper into the key phenomena of how macrophage-derived Exo delivering BRCA1 protein affects VSMCs function, we established an in vitro co-culture system. The macrophage cell line Ana-1 was stimulated with 50 ng/mL LPS and 40 ng/mL IFN-γ for 24 h to obtain M1 macrophages. These macrophages were then co-cultured with SMCs, with M0 or M1 macrophages in the upper chamber and SMCs in the lower chamber. Prior to co-culture, M1 macrophages were pre-treated with 10 μM GW4869 for 8 h to inhibit exosome release. BRCA1 protein expression and cell proliferation were then assessed in the M0 + SMC group, M1 + SMC group, and M1 + SMC + GW4869 group. The M1 + SMC group demonstrated the highest ratio of positive SMC cells in the study findings (Figure S5D). Additionally,

BRCA1 protein expression in the M1 + SMC group was substantially higher than in the control group, and this expression was markedly inhibited after the addition of the GW4869 inhibitor (Figure S5E). These findings provide evidence of direct BRCA1 transfer from M1 macrophage-derived Exo to target cells.

In our previous studies, we confirmed an increased level of BRCA1 protein in M1 macrophages and their derived Exo. To validate the in vivo transmission of activated M1 macrophages to target cells within an animal model, we injected BRCA1-modified DiI-labeled Exo into a carotid artery injury mouse model and subsequently conducted various analyses on the treated tissue samples. Observations of exosome distribution across various organs revealed a predominant concentration within the heart (Fig. 6A). Furthermore, immunofluorescence analysis of specific cell types showed notable colocalization in both vascular endothelium and vascular smooth muscle cells (Fig. 6B). These findings indicate that M1 macrophage-derived Exo primarily localizes within cardiac cells post-injection and exhibits colocalization with smooth muscle cells in the heart, demonstrating the in vivo exosome delivery process.

Subsequently, H&E staining was performed on carotid artery tissues to observe pathological changes, specifically the formation of neointima, directly illustrating the thickening effect mediated by BRCA1 delivered through M1-derived Exo. Compared to the Surgery group, the Exo.NC group exhibited significant intimal thickening. In contrast, the Exo. shBRCA1 group suppressed neointima formation relative to the Exo.NC group, while the Exo.oeBRCA1 group promoted it compared to the Exo.vehicle group (Fig. 6C). The IHC staining results demonstrated that contrasted against the Surgery group, αSMA (SMC marker) expression increased in the Exo.NC group; as opposed to the Exo.NC group, the αSMA expression indicated a decline in the Exo.shBRCA1 group. When contrasted with the Exo.Vehicle group, αSMA expression was upregulated in the Exo. oeBRCA1 group (Fig. 6D-E). Immunofluorescence staining revealed SMC proliferation, showing that contrasted against the Surgery group, the expression of αSMA + Ki67 + co-located cells increased in the Exo.NC group; contrasted with the Exo.NC group, the expression of αSMA + Ki67 + co-located cells decreased in the Exo.shBRCA1 group (Fig. 6F-G). The importance of BRCA1 in controlling the proliferation of SMCs is prominently emphasized.

In summary, the experimental results from this section demonstrate the critical role of Exo derived from M1 macrophages in delivering BRCA1 during the cardiovascular system remodeling process, especially in aspects such as neointima formation and the proliferation and migration of SMC.

Exo.siBRCA1 mitigates coronary artery atherosclerosis

Subsequently, we conducted an in vivo therapeutic study targeting CAD (CAD) atherosclerosis to examine the potential regulatory impact of BRCA1-modified Exo in the pathological progression of affected patients. Using a high-fat diet-induced $ApoE^{-/-}$ mouse model, we tracked the dynamic expression pattern of BRCA1 during the development of coronary lesions. Western blot analysis exhibited substantial variations in BRCA1 expression levels in the carotid artery and heart tissues at various time points of the model establishment, showing a gradual increase over time (Figure S6A-B). Immunofluorescence staining further demonstrated the expression of $BRCA1^{+}CD86^{+}CD80^{+}$ cells in the endocardial tissues and carotid arteries of $ApoE^{-/-}$ mice at early (12 weeks) and late (20 weeks) stages. A remarkable elevation in the amount of $BRCA1^{+}CD86^{+}CD80^{+}$ positive cells was observed in the late stage versus the early stage (Figure S6C-D). The fluorescence intensity in early and late stages progressively increased, compared to the weaker background fluorescence levels (Figure S6C-D).

Results indicate that as atherosclerosis worsens, BRCA1 expression gradually increases, along with the proportion of M1 macrophages. This validates our previous hypothesis, confirming the close link between BRCA1 delivery by M1 macrophage-derived Exo and the progression of CAD atherosclerosis.

Next, to evaluate the therapeutic effect of BRCA1-silenced Exo, we loaded BRCA1-inhibited siRNA into Exo in vitro and administered them to the $ApoE^{-/-}$ atherosclerosis mouse model for intervention (Fig. 7A). Initially, the experiment observed the pathological condition of the entire aorta and its branches in each group of $ApoE^{-/-}$ mice. Compared with the $ApoE^{-/-}$ group, there was no significant change in the atherosclerotic plaque in the Exo.NC group. However, compared with the Exo.NC group,

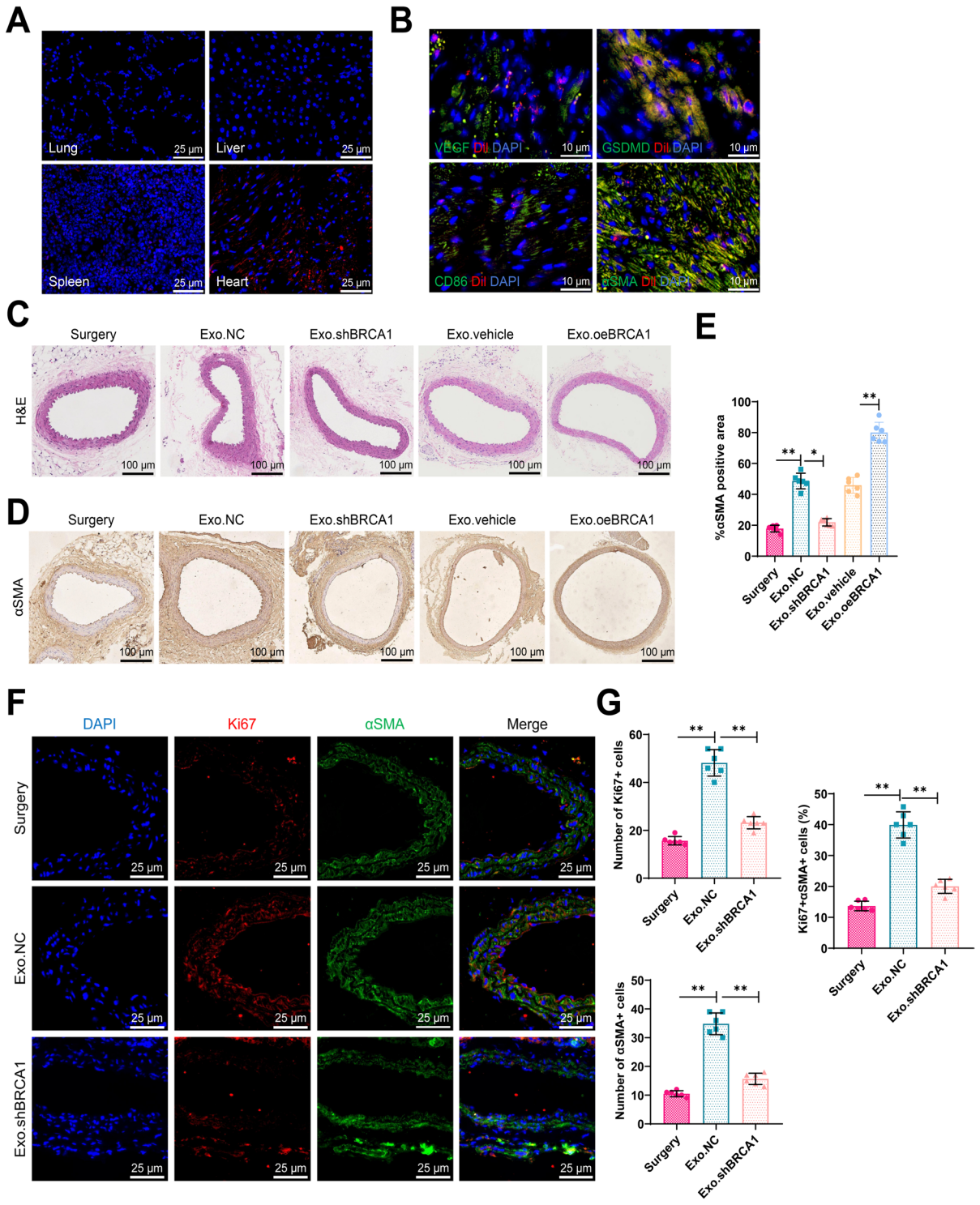

the Exo.siBRCA1 group significantly reduced atherosclerotic plaque (Figs. 7B-C). Additionally, H&E and Oil Red O staining results also showed that, compared with the ApoE$^{-/-}$ group and the Exo.NC group, the lesion area in the Exo.siBRCA1 group was significantly reduced (Figs. 7D-E). Meanwhile, the levels of

◂**Fig. 6** Exo from Macrophages Delivering BRCA1 Influence SMC Cell Function. Note: (A) Immunofluorescence analysis of the distribution in the heart, liver, spleen, and lungs after exosome injection in an animal model, scale bar = 25 μm; (B) Immunofluorescence analysis of cell types with exosome distribution, scale bar = 25 μm; (C) H&E staining of carotid artery tissues from various mouse groups, scale bar = 200 μm; (D-E) IHC staining for αSMA expression, a smooth muscle cell marker, in carotid artery tissues of mouse groups, Scale bar = 100 μm; (F-G) Immunofluorescence staining to assess smooth muscle cell proliferation in carotid artery tissues, αSMA indicates smooth muscle cells, Ki67 indicates proliferating cells, DAPI indicates nuclei, white arrows point to αSMA + Ki67 + double-positive cells, scale bar = 25 μm. ***$P < 0.001$, **$P < 0.01$, *$P < 0.05$, $^{ns}P > 0.05$, animal experiment n = 6

TC, TG, and LDL-C in peripheral blood were measured in each group of CAD mice. The results indicated that, compared with the ApoE$^{-/-}$ group and the Exo.NC group, the Exo.siBRCA1 group significantly reduced the expression of TC, TG, and LDL-C (Figures S7A-C).

In addition, the SNP near the ILRUN gene, which has a ubiquitin-associated domain and an NBR1-like domain adjacent to the BRCA1 gene, has been shown to be significantly associated with plasma lipid profiles and CAD. Studies have identified ILRUN as a novel lipid metabolism regulator that promotes liver lipoprotein production (Bi et al. 2020). Additional studies indicate a connection between BRCA1 and acetyl-CoA carboxylase alpha (ACCA) via its tandem BRCT domains, influencing lipid synthesis by inhibiting the dephosphorylation of P-ACCA (Moreau et al. 2006). Therefore, we speculate that the interaction between BRCA1 and ACCA may have an impact on lipid metabolism. In summary, M1 macrophage-derived Exo likely influences atherosclerotic progression by delivering BRCA1.

Using IHC staining, the experiment further analyzed the expression levels of the pyroptosis-related protein GSDMD. The results showed that, compared with the ApoE$^{-/-}$ and Exo.NC groups, the expression level of GSDMD was significantly reduced in the Exo.siBRCA1 group (Fig. 7F). The pyroptosis levels in cardiomyocytes also showed a similar trend (Fig. 7G), with a significantly lower proportion of pyroptotic cells in the Exo.siBRCA1 group compared to the ApoE$^{-/-}$ and Exo.NC groups. Western blot results demonstrated that the expression levels of GSDMD, Caspase-1, and Caspase-4 in the Exo.siBRCA1 group were markedly reduced compared with the ApoE$^{-/-}$ and Exo.NC groups (Fig. 7H). qRT-PCR was used to detect BRCA1 mRNA expression levels in M1 macrophages before and after the intervention, showing that the intervention significantly inhibited BRCA1 mRNA expression in M1 macrophages compared to the negative control group (Fig. 7I).

The experiment further assessed the inflammatory response levels by measuring the expression of inflammatory cytokines IL-1β, IL-6, and IL-18 in the peripheral blood of each mouse group. Results indicated that the Exo.siBRCA1 group had significantly lower levels of these cytokines compared to both the ApoE$^{-/-}$ and Exo.NC groups (Figures S7D-F), suggesting that BRCA1-silenced Exo can effectively reduce inflammatory responses in cardiovascular disease. We hypothesize that the protective mechanism of si-Exo treatment mainly involves exosome delivery of siRNA targeting BRCA1 silencing. This approach subsequently influences the non-canonical pyroptosis pathway in cardiomyocytes activated by the inflammatory response.

In summary, this segment of the research found that Exo derived from M1 macrophages delivering BRCA1 can promote the progression of atherosclerosis, providing significant scientific evidence for developing therapeutic strategies against coronary artery atherosclerosis.

Discussion

CAD, a leading cause of cardiovascular mortality globally, has always been a focal point in medical research due to its complex pathogenesis (Olsen et al. 2022, Makover et al. 2022; Velusamy et al. 2023). Cardiomyocyte apoptosis and inflammatory responses play pivotal roles in the progression of CAD (Wu et al. 2022a, b, Mosquera et al. 2023, Fan et al. 2022). Recent advancements in molecular biology have shifted research attention towards immune cells, particularly M1 macrophages and their secreted Exo, and their roles in cardiovascular diseases (Mohd Idrus et al. 2021; Li et al. 2021a, b). These Exo, critical for intercellular communication, carry various biomolecules, including proteins and RNA, influencing the behavior and function of recipient cells (Mao et al. 2021; Kalluri and McAndrews 2023; Lai et al. 2022). Investigating specific molecules within M1

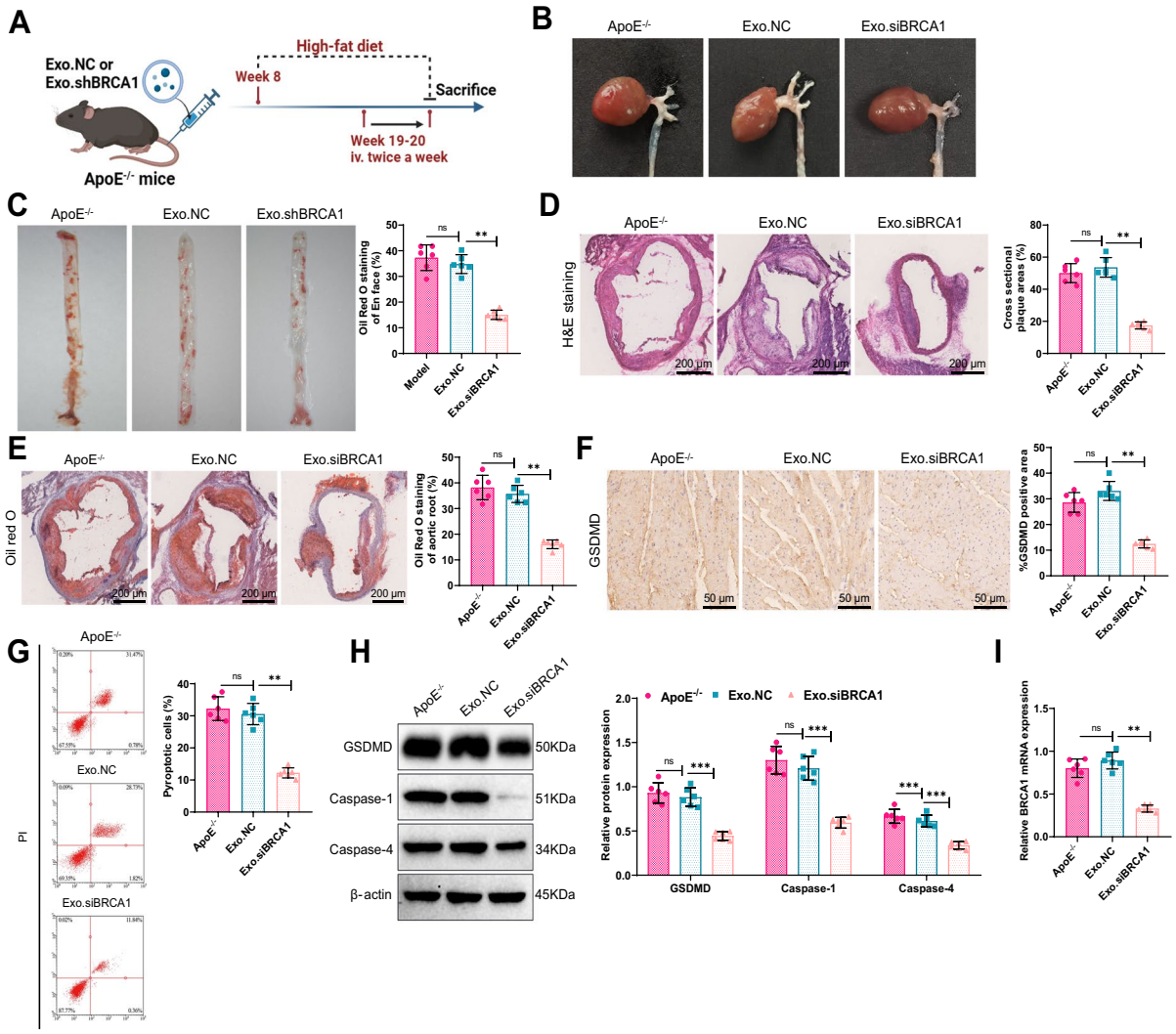

Fig. 7 Mechanistic Study of BRCA1-Modified Exo in Coronary Artery Atherosclerosis. Note: (A) Schematic of atherosclerosis model in 8-week-old ApoE$^{-/-}$ mice fed a high-fat diet for 12 weeks and treated with BRCA1-modified Exo; (B) Representative images of atherosclerotic plaques (yellow arrows) in the aorta and its branches of mouse groups; (C) Representative images and quantification of Oil red O staining in the entire aorta lesion area of mouse groups; (D) Representative images and cross-sectional plaque area statistics of aortic root H&E staining in mouse groups, Scale bar = 200 μm; (E) Representative images and analysis of Oil red O staining in the aortic root of mouse groups, Scale bar = 200 μm; (F) IHC staining for GSMDM expression in cardiac tissues of mouse groups, Scale bar = 50 μm; (G) Flow cytometry analysis of the proportion of pyroptosis in cardiomyocytes of model, negative control, and BRCA1-silenced groups, with flow cytometry results and statistical bar graphs displayed; (H) Western blot analysis of the expression of GSDMD, Caspase-1, and Caspase-4 in the heart tissues of each group of mice; (I) qRT-PCR analysis of BRCA1 mRNA expression levels in M1 macrophages before and after interference treatment. $^{**}P < 0.01$, $^{*}P < 0.05$, animal experiment n = 6

macrophage-derived Exo, such as BRCA1, and their impact on cardiomyocyte apoptosis and the CAD process can deepen our understanding of CAD pathophysiology and potentially guide the development of new therapeutic strategies.

Previous research has predominantly concentrated on examining the functions of cardiomyocyte apoptosis and inflammation in CAD, with relatively less attention given to M1 macrophages and their Exo (Jiang et al. 2021; Xiang et al. 2024; Xiao et al. 2022).

Although existing literature highlights the significant role of macrophages in cardiovascular diseases, these studies often lack single-cell resolution and clarity on the functions of specific molecules within their Exo. This study innovates by utilizing single-cell multi-omics techniques to precisely identify the role of BRCA1 in M1 macrophage-derived Exo in promoting cardiomyocyte apoptosis, offering new molecular mechanisms for the interaction between M1 macrophages and cardiomyocytes. Moreover, this research provides more direct evidence of BRCA1's influence on CAD advancement through an integrated application of bioinformatics and molecular biology techniques, surpassing previous research in depth and specificity.

A highlight of this study is the application of single-cell multi-omics analysis techniques, allowing for the observation of complex interactions between macrophages and cardiomyocytes at the single-cell level. The application of scRNA-seq enabled the characterization of both M1 macrophages and cardiomyocytes at the cellular level, unveiling the pivotal function of BRCA1 in this context. Compared to traditional bulk data, single-cell analysis offers unprecedented precision and detail, capturing subtle changes in intercellular communication and providing the research with an unparalleled level of detail. By comprehensively utilizing advanced bioinformatics techniques such as pseudotime analysis and WGCNA (Dai et al. 2021; Chen et al. 2023), the identification of key genes and signaling pathways closely associated with cardiomyocyte pyroptosis was a significant achievement in this research. The application of these techniques not only enhanced the precision of the research but also provided powerful tools for understanding the molecular mechanisms of complex diseases. In particular, WGCNA, by analyzing patterns in gene expression data, helped us pinpoint gene networks highly related to cardiomyocyte pyroptosis, guiding subsequent experimental research.

The existing research indicates a co-occurrence of hypercholesterolemia and TET2 deficiency in the activation pathway of the NLRP3 inflammasome. This pathway is influenced by the activation of JNK1 and the NLRP3 deubiquitination facilitated by BRCC3, holding significance for potential therapeutic interventions to deter cardiovascular disease in individuals with TET2 CH. JNK1 signaling augmentation leads to NLRP3 deubiquitination and activation by the deubiquitinase BRCC3 (BRCA1/BRCA2-containing complex subunit 3) (Yalcinkaya et al. 2023). This provides evidence that BRCA family proteins may be related to cardiovascular disease. Our research primarily focused on elucidating the role of BRCA1 in atherosclerosis and cardiomyocyte pyroptosis, revealing that BRCA1 in M1 macrophage-derived Exo promotes cardiomyocyte pyroptosis through specific signaling pathways. Two key pathways have been identified in pyroptosis research: the classical and non-classical pathways (Liu et al. 2021). GSDMD cleavage is the key molecular mechanism of pyroptosis, where GSDMD acts as the direct effector of pyroptosis induced by inflammatory caspases. The classical pyroptosis pathway relies on caspase-1, whereas the non-classical pyroptosis pathway is triggered by caspase-4/5/11 upon recognition of cytosolic lipopolysaccharide. In this pathway, the cleavage of IL-1β and IL-18 precursors is dependent on caspase-1 (Frank and Vince 2018). Our results showed a significant increase in IL-18, IL-1β, GSDMD, Caspase-1, and Caspase-4 levels in the BRCA1-overexpressing group, suggesting that BRCA1 influences cell activity through the non-classical pyroptosis pathway. Further experiments confirmed the key role of BRCA1 in cardiomyocyte pyroptosis, with BRCA1-modified Exo exacerbating the inflammatory response. Studies have shown that BRCA1 can regulate the PI3K-Akt signaling pathway (Kim et al. 2021). In cardiomyocytes, activated Akt inhibits glycogen synthase kinase-3β (GSK-3β), and this inhibition promotes cell survival and proliferation. Akt also regulates the mTOR (mammalian target of rapamycin) pathway, which is a key regulator of cell growth and proliferation, promoting protein synthesis to support cardiomyocyte growth and proliferation. BRCA1 interacts with PI3K and affects PI3K activity. Akt, as a downstream molecule of PI3K, interacts with GSK-3β and mTOR. For example, Akt's phosphorylation of GSK-3β alters its activity, and there is a feedback regulation between Akt and mTOR. Akt can activate mTOR, and mTOR can influence upstream regulators of the PI3K-Akt pathway, thereby modulating Akt activity (Kim et al. 2021; Gao et al. 2017). Further exploration of these signaling pathways will be conducted in subsequent research.

The findings of this study not only provide new scientific insights but also have important clinical implications. Current drugs targeting BRCA1 primarily focus on the DNA repair defects caused by BRCA1/2

mutations, which have led to the development of cytotoxic drugs targeting DNA, such as cisplatin and carboplatin. In addition, poly(ADP-ribose) polymerase (PARP) inhibitors, which also hinder DNA repair, should be more sensitive (Nie et al. 2023). The findings in this study not only enrich our understanding of BRCA1's biological functions but also provide a new perspective on the role of cardiomyocyte pyroptosis in CAD. At the same time, we identify potential therapeutic targets, laying a theoretical foundation for the development of new drugs. Therefore, theoretically, targeting BRCA1 or its related signaling pathways may help reduce cardiomyocyte pyroptosis, thereby slowing or halting the progression of CAD. In the future, gene therapy could be designed to target the positive correlation between BRCA1 and the inflammatory response. Furthermore, the development of small molecule inhibitors or immunotherapies targeting BRCA1 and related pathways may also be helpful. Regarding the long-term effects of BRCA1 on CAD progression, further longitudinal studies are required to assess the chronic impact of BRCA1 regulation.

However, due to the widespread effects of BRCA1, potential side effects and nonspecific actions still need to be explored and validated. Since BRCA1 is a well-known tumor suppressor gene, its mutation or dysfunction significantly increases the risk of breast cancer, ovarian cancer, and other cancers (Takaoka and Miki 2017; Sánchez-Lorenzo et al. 2022; Oubaddou et al. 2023). For CAD patients, if BRCA1-related cancer risks are present, CAD treatments (such as certain drugs or heart interventions) may interfere with cancer therapies. For instance, radiotherapy or chemotherapy may impose additional toxic effects on the heart, exacerbating the cardiac burden in CAD patients (Chen et al. 2006). Additionally, cancer-induced physical wasting and inflammation could interact with CAD, worsening the patient's condition. Considering BRCA1's potential role in CAD progression, gene therapy targeting BRCA1 might emerge in the future. However, gene therapy itself has numerous potential risks. For example, correcting BRCA1 gene expression abnormalities may provoke immune responses against the gene delivery vectors, leading to inflammation, allergic reactions, and other adverse events. Moreover, gene therapy's targeting and efficacy still face many challenges. If BRCA1 expression cannot be precisely regulated, it could cause other cellular dysfunctions or even lead to new cardiovascular problems and nonspecific effects. These challenges need to be considered in future research.

This study also explored the therapeutic effects of exosome-mediated delivery of shBRCA1 and confirmed that BRCA1 silencing inhibited pyroptosis in cardiomyocytes. In the future, exosome-mediated gene delivery therapies could be widely applied, combined with current lifestyle modifications (such as smoking cessation, reduced alcohol intake, low-fat, low-salt diet, regular exercise, weight control, etc.) and pharmacological treatments to improve atherosclerosis therapy. The successful implementation of this strategy may have a significant impact on the treatment of CAD patients. In conclusion, we found that M1 macrophage-derived Exo exacerbates cardiomyocyte pyroptosis through the transfer of BRCA1, thereby promoting the development of coronary artery atherosclerosis. This discovery provides new molecular targets for CAD treatment and offers the potential for developing new therapeutic strategies.

Despite the important findings of this study, some limitations exist. For example, the experiments were mainly based on animal models, and the cell lines used were murine-derived cardiac and macrophage cells, which may introduce species-specific bias. Our conclusions and specific experimental results need to be further validated in human samples by replacing them with humanized cell lines and conducting targeted discussions and in-depth studies using patient samples from relevant diseases. Additionally, this study mainly focused on M1 macrophage-derived Exo, neglecting the potential roles of Exo from other cell types such as endothelial cells, vascular smooth muscle cells, or stem cells, which represents a limitation of the study. Future research will extend the exploration of Exo from other cell types. Furthermore, studies have shown that AS mice on a high-fat diet receiving 12 weeks of intravenous injection of Exo derived from mesenchymal stem cells significantly reduced plaque area and macrophage infiltration, and further confirmed that mesenchymal stem cell-derived Exo promotes M2 macrophage polarization in plaques via the miR-let7 pathway (Li et al. 2019). Therefore, this study primarily discusses M1 macrophage-derived Exo while overlooking the role of Exo from other cell types in CAD and lacks an evaluation of the long-term therapeutic effects of BRCA1 in CAD. Additionally, the MI intervention in the dataset may introduce limitations on the scope of this study. The mechanism of

BRCA1 in CAD is not yet fully elucidated, and more research is needed to explore its specific functions in different cell types. Exo is known to carry numerous signaling molecules; however, we did not examine cytokine levels in the Exo (such as IL6, TNFα, IL1β). We plan to explore these factors in future studies and eliminate any interference from background cytokine levels. Future studies could deepen our understanding of CAD pathology by increasing sample sizes, using human samples for validation, and exploring the downstream signaling pathways of BRCA1, thus providing more targets for clinical treatment.

Acknowledgements None.

Author contributions Hairui Yu and Dong Wei conceived and designed the study. Weiqian Liao and Xiaoming Shang performed the experiments. Dandan Li and Chunzhao Liu conducted data analysis and interpretation. Qimei Deng contributed to the single-cell RNA-seq data acquisition. Haiquan Huangfu supervised the project and revised the manuscript. All authors contributed to the drafting and editing of the manuscript and approved the final version for submission..

Funding This study was supported by 2023 Luohu District Soft Science Program (No: LX202302068; No: LX202302082), Research Project of Guangdong Provincial Administration of Traditional Chinese Medicine(No.20251323) and Supported by Sanming Project of Medicine in Shenzhen (No. SZZYSM202401018).

Data availability All data can be provided as needed.

Declarations

Ethical statement All animal experiments were approved by the Animal Ethics Committee of Shenzhen Hospital of Shanghai University of Traditional Chinese Medicine(2023-LHQZYYYXLL-KY-133).

Conflict of interest The authors declare no competing interests.

Open Access This article is licensed under a Creative Commons Attribution-NonCommercial-NoDerivatives 4.0 International License, which permits any non-commercial use, sharing, distribution and reproduction in any medium or format, as long as you give appropriate credit to the original author(s) and the source, provide a link to the Creative Commons licence, and indicate if you modified the licensed material. You do not have permission under this licence to share adapted material derived from this article or parts of it. The images or other third party material in this article are included in the article's Creative Commons licence, unless indicated otherwise in a credit line to the material. If material is not included in the article's Creative Commons licence and your intended use is not permitted by statutory regulation or exceeds the permitted use, you will need to obtain permission directly from the copyright holder. To view a copy of this licence, visit http://creativecommons.org/licenses/by-nc-nd/4.0/.

References

Alsiary R, Brownhill SC, Brüning-Richardson A, Hutson R, Griffin N, Morrison EE, et al. Expression analysis of the MCPH1/BRIT1 and BRCA1 tumor suppressor genes and telomerase splice variants in epithelial ovarian cancer [Internet]. Gene. Elsevier BV; 2018 [cited 2025 Jan 22]. p. 34–44. Available from: https://doi.org/10.1016/j.gene.2018.05.113

Arya SB, Chen S, Jordan-Javed F, Parent CA. Ceramide-rich microdomains facilitate nuclear envelope budding for non-conventional exosome formation [Internet]. Nat Cell Biol. Springer Science and Business Media LLC; 2022 [cited 2025 Jan 22]. p. 1019–28. Available from: https://doi.org/10.1038/s41556-022-00934-8

Batulan Z, Maarouf N, Shrivastava V, O'Brien E. Prophylactic salpingo-oophorectomy & surgical menopause for inherited risks of cancer: the need to identify biomarkers to assess the theoretical risk of premature coronary artery disease [Internet]. womens midlife health. Springer Science and Business Media LLC; 2018 [cited 2025 Jan 22]. Available from: https://doi.org/10.1186/s40695-018-0037-y

Benincasa G, Suades R, Padró T, Badimon L, Napoli C. Bioinformatic platforms for clinical stratification of natural history of atherosclerotic cardiovascular diseases [Internet]. European Heart Journal - Cardiovascular Pharmacotherapy. Oxford University Press (OUP); 2023 [cited 2025 Jan 22]. p. 758–69. Available from: https://doi.org/10.1093/ehjcvp/pvad059

Bi X, Kuwano T, Lee PC, Millar JS, Li L, Shen Y, et al. ILRUN, a Human Plasma Lipid GWAS Locus, Regulates Lipoprotein Metabolism in Mice [Internet]. Circulation Research. Ovid Technologies (Wolters Kluwer Health); 2020 [cited 2025 Jan 22]. p. 1347–61. Available from: https://doi.org/10.1161/circresaha.120.317175

Bu T, Li Z, Hou Y, Sun W, Zhang R, Zhao L, et al. Exosome-mediated delivery of inflammation-responsive Il-10 mRNA for controlled atherosclerosis treatment [Internet]. Theranostics. Ivyspring International Publisher; 2021 [cited 2025 Jan 22]. p. 9988–10000. Available from: https://doi.org/10.7150/thno.64229

Del Buono MG, Moroni F, Montone RA, Azzalini L, Sanna T, Abbate A. Ischemic Cardiomyopathy and Heart Failure After Acute Myocardial Infarction [Internet]. Curr Cardiol Rep. Springer Science and Business Media LLC; 2022 [cited 2025 Jan 22]. p. 1505–15. Available from: https://doi.org/10.1007/s11886-022-01766-6

Butler A, Hoffman P, Smibert P, Papalexi E, Satija R. Integrating single-cell transcriptomic data across different conditions, technologies, and species [Internet]. Nat Biotechnol. Springer Science and Business Media LLC; 2018

[cited 2025 Jan 22]. p. 411–20. Available from: https://doi.org/10.1038/nbt.4096

Cai S, Zhao M, Zhou B, Yoshii A, Bugg D, Villet O, et al. Mitochondrial dysfunction in macrophages promotes inflammation and suppresses repair after myocardial infarction [Internet]. Journal of Clinical Investigation. American Society for Clinical Investigation; 2023 [cited 2025 Jan 22]. Available from: https://doi.org/10.1172/jci159498

Chang S-N, Chen J-J, Wu J-H, Chung Y-T, Chen J-W, Chiu C-H, et al. Association between Exosomal miRNAs and Coronary Artery Disease by Next-Generation Sequencing [Internet]. Cells. MDPI AG; 2021 [cited 2025 Jan 22]. p. 98. Available from: https://doi.org/10.3390/cells11010098

Chen G-C, Guan L-S, Yu J-H, Li G-C, Choi Kim H-R, Wang Z-Y. Rb-Associated Protein 46 (RbAp46) Inhibits Transcriptional Transactivation Mediated by BRCA1 [Internet]. Biochemical and Biophysical Research Communications. Elsevier BV; 2001 [cited 2025 Jan 22]. p. 507–14. Available from: https://doi.org/10.1006/bbrc.2001.5003

Chen X, Arciero CA, Godwin AK. BRCA1-associated complexes: new targets to overcome breast cancer radiation resistance [Internet]. Expert Review of Anticancer Therapy. Informa UK Limited; 2006 [cited 2025 Jan 22]. p. 187–96. Available from: https://doi.org/10.1586/14737140.6.2.187

Chen S, Morine Y, Tokuda K, Yamada S, Saito Y, Nishi M, et al. Cancer-associated fibroblast-induced M2-polarized macrophages promote hepatocellular carcinoma progression via the plasminogen activator inhibitor-1 pathway [Internet]. Int J Oncol. Spandidos Publications; 2021 [cited 2025 Jan 22]. Available from: https://doi.org/10.3892/ijo.2021.5239

Chen D, Wang H, Cai X. Curcumin interferes with sepsis-induced cardiomyocyte apoptosis via TLR1 inhibition [Internet]. Revista Portuguesa de Cardiologia. Elsevier BV; 2023 [cited 2025 Jan 22]. p. 209–21. Available from: https://doi.org/10.1016/j.repc.2023.01.013

Chen R, Zhang H, Tang B, Luo Y, Yang Y, Zhong X, et al. Macrophages in cardiovascular diseases: molecular mechanisms and therapeutic targets [Internet]. Sig Transduct Target Ther. Springer Science and Business Media LLC; 2024 [cited 2025 Jan 22]. Available from: https://doi.org/10.1038/s41392-024-01840-1

Cheng P, Li S, Chen H. Macrophages in Lung Injury, Repair, and Fibrosis [Internet]. Cells. MDPI AG; 2021 [cited 2025 Jan 22]. p. 436. Available from: https://doi.org/10.3390/cells10020436

Crossley MP, Song C, Bocek MJ, Choi J-H, Kousouros JN, Sathirachinda A, et al. R-loop-derived cytoplasmic RNA–DNA hybrids activate an immune response [Internet]. Nature. Springer Science and Business Media LLC; 2022 [cited 2025 Jan 22]. p. 187–94. Available from: https://doi.org/10.1038/s41586-022-05545-9

Dai L, Xie Y, Zhang W, Zhong X, Wang M, Jiang H, et al. Weighted Gene Co-Expression Network Analysis Identifies ANGPTL4 as a Key Regulator in Diabetic Cardiomyopathy via FAK/SIRT3/ROS Pathway in Cardiomyocyte [Internet]. Front. Endocrinol. Frontiers Media SA; 2021 [cited 2025 Jan 22]. Available from: https://doi.org/10.3389/fendo.2021.705154

Dalen JE, Alpert JS, Goldberg RJ, Weinstein RS. The Epidemic of the 20th Century: Coronary Heart Disease [Internet]. The American Journal of Medicine. Elsevier BV; 2014 [cited 2025 Jan 22]. p. 807–12. Available from: https://doi.org/10.1016/j.amjmed.2014.04.015

Dawson LP, Lum M, Nerleker N, Nicholls SJ, Layland J. Coronary Atherosclerotic Plaque Regression [Internet]. Journal of the American College of Cardiology. Elsevier BV; 2022 [cited 2025 Jan 22]. p. 66–82. Available from: https://doi.org/10.1016/j.jacc.2021.10.035

Doenst T, Thiele H, Haasenritter J, Wahlers T, Massberg S, Haverich A. The treatment of coronary artery disease—current status six decades after the first bypass operation [Internet]. Deutsches Ärzteblatt international. Deutscher Arzte-Verlag GmbH; 2022 [cited 2025 Jan 22]. Available from: https://doi.org/10.3238/arztebl.m2022.0277

Duggan JP, Peters AS, Trachiotis GD, Antevil JL. Epidemiology of Coronary Artery Disease [Internet]. Surgical Clinics of North America. Elsevier BV; 2022 [cited 2025 Jan 22]. p. 499–516. Available from: https://doi.org/10.1016/j.suc.2022.01.007

Fan X, Yang G, Kowitz J, Akin I, Zhou X, El-Battrawy I. Takotsubo Syndrome: Translational Implications and Pathomechanisms [Internet]. IJMS. MDPI AG; 2022 [cited 2025 Jan 22]. p. 1951. Available from: https://doi.org/10.3390/ijms23041951

Feng X, Du M, Li S, Zhang Y, Ding J, Wang J, et al. Hydroxysafflor yellow A regulates lymphangiogenesis and inflammation via the inhibition of PI3K on regulating AKT/mTOR and NF-κB pathway in macrophages to reduce atherosclerosis in ApoE-/- mice [Internet]. Phytomedicine. Elsevier BV; 2023 [cited 2025 Jan 22]. p. 154684. Available from: https://doi.org/10.1016/j.phymed.2023.154684

Fioranelli M, Bottaccioli AG, Bottaccioli F, Bianchi M, Rovesti M, Roccia MG. Stress and Inflammation in Coronary Artery Disease: A Review Psychoneuroendocrineimmunology-Based [Internet]. Front. Immunol. Frontiers Media SA; 2018 [cited 2025 Jan 22]. Available from: https://doi.org/10.3389/fimmu.2018.02031

Frank D, Vince JE. Pyroptosis versus necroptosis: similarities, differences, and crosstalk [Internet]. Cell Death Differ. Springer Science and Business Media LLC; 2018 [cited 2025 Jan 22]. p. 99–114. Available from: https://doi.org/10.1038/s41418-018-0212-6

Gao S, Sun H, Cheng C, Wang G. BRCA1-Associated Protein-1 Suppresses Osteosarcoma Cell Proliferation and Migration Through Regulation PI3K/Akt Pathway [Internet]. DNA and Cell Biology. Mary Ann Liebert Inc; 2017 [cited 2025 Jan 22]. p. 386–93. Available from: https://doi.org/10.1089/dna.2016.3579

Gao X, Bao W, Bai J, Fan K, Li L, Li Y. UHMK1 aids colorectal cancer cell proliferation and chemoresistance through augmenting IL-6/STAT3 signaling [Internet]. Cell Death Dis. Springer Science and Business Media LLC; 2022 [cited 2025 Jan 22]. Available from: https://doi.org/10.1038/s41419-022-04877-8

Goldsborough E III, Osuji N, Blaha MJ. Assessment of Cardiovascular Disease Risk [Internet]. Endocrinology and

Metabolism Clinics of North America. Elsevier BV; 2022 [cited 2025 Jan 22]. p. 483–509. Available from: https://doi.org/10.1016/j.ecl.2022.02.005

Habibi J, DeMarco VG, Hulse JL, Hayden MR, Whaley-Connell A, Hill MA, et al. Inhibition of sphingomyelinase attenuates diet – Induced increases in aortic stiffness [Internet]. Journal of Molecular and Cellular Cardiology. Elsevier BV; 2022 [cited 2025 Jan 22]. p. 32–9. Available from: https://doi.org/10.1016/j.yjmcc.2022.03.006

Hao Y, Hao S, Andersen-Nissen E, Mauck WM III, Zheng S, Butler A, et al. Integrated analysis of multimodal single-cell data [Internet]. Cell. Elsevier BV; 2021 [cited 2025 Jan 22]. p. 3573–3587.e29. Available from: https://doi.org/10.1016/j.cell.2021.04.048

Incorvaia L, Badalamenti G, Novo G, Gori S, Cortesi L, Brando C, et al. Anthracycline-related cardiotoxicity in patients with breast cancer harboring mutational signature of homologous recombination deficiency (HRD) [Internet]. ESMO Open. Elsevier BV; 2024 [cited 2025 Jan 22]. p. 102196. Available from: https://doi.org/10.1016/j.esmoop.2023.102196

Indolfi C, Iaconetti C, Gareri C, Polimeni A, De Rosa S. Non-coding RNAs in vascular remodeling and restenosis [Internet]. Vascular Pharmacology. Elsevier BV; 2019 [cited 2025 Jan 22]. p. 49–63. Available from: https://doi.org/10.1016/j.vph.2018.10.006

Janakiraman V, Sudhan M, Wani A, Ahmad SF, Nadeem A, Sharma A, et al. Pharmacoscreening, molecular dynamics, and quantum mechanics of inermin from Panax ginseng: a crucial molecule inhibiting exosomal protein target associated with coronary artery disease progression [Internet]. PeerJ. PeerJ; 2023 [cited 2025 Jan 22]. p. e16481. Available from: https://doi.org/10.7717/peerj.16481

Jia Z, Liu Q, Xie Y, Wei J, Sun X, Meng F, et al. Klotho/FGF23 Axis Regulates Cardiomyocyte Apoptosis and Cytokine Release through ERK/MAPK Pathway [Internet]. Cardiovasc Toxicol. Springer Science and Business Media LLC; 2023 [cited 2025 Jan 22]. p. 317–28. Available from: https://doi.org/10.1007/s12012-023-09805-6

Jiang Y, Sun S-J, Zhen Z, Wei R, Zhang N, Liao S-Y, et al. Myocardial repair of bioengineered cardiac patches with decellularized placental scaffold and human-induced pluripotent stem cells in a rat model of myocardial infarction [Internet]. Stem Cell Res Ther. Springer Science and Business Media LLC; 2021 [cited 2025 Jan 22]. Available from: https://doi.org/10.1186/s13287-020-02066-y

Kalluri R, McAndrews KM. The role of extracellular vesicles in cancer [Internet]. Cell. Elsevier BV; 2023 [cited 2025 Jan 22]. p. 1610–26. Available from: https://doi.org/10.1016/j.cell.2023.03.010

Kim M, Park J, Bouhaddou M, Kim K, Rojc A, Modak M, et al. A protein interaction landscape of breast cancer [Internet]. Science. American Association for the Advancement of Science (AAAS); 2021 [cited 2025 Jan 22]. Available from: https://doi.org/10.1126/science.abf3066

Kim C, Wang X-D, Jang S, Yu Y. PARP1 inhibitors induce pyroptosis via caspase 3-mediated gasdermin E cleavage [Internet]. Biochemical and Biophysical Research Communications. Elsevier BV; 2023 [cited 2025 Jan 22]. p. 78–85. Available from: https://doi.org/10.1016/j.bbrc.2023.01.055

Kishore A, Petrek M. Roles of Macrophage Polarization and Macrophage-Derived miRNAs in Pulmonary Fibrosis [Internet]. Front. Immunol. Frontiers Media SA; 2021 [cited 2025 Jan 22]. Available from: https://doi.org/10.3389/fimmu.2021.678457

Kluszczynska K, Czyz M. Extracellular Vesicles-Based Cell-Cell Communication in Melanoma: New Perspectives in Diagnostics and Therapy [Internet]. IJMS. MDPI AG; 2023 [cited 2025 Jan 22]. p. 965. Available from: https://doi.org/10.3390/ijms24020965

Kong Y, Akatsuka S, Motooka Y, Zheng H, Cheng Z, Shiraki Y, et al. BRCA1 haploinsufficiency promotes chromosomal amplification under Fenton reaction-based carcinogenesis through ferroptosis-resistance [Internet]. Redox Biology. Elsevier BV; 2022 [cited 2025 Jan 22]. p. 102356. Available from: https://doi.org/10.1016/j.redox.2022.102356

Lai Z-Z, Wang Y, Zhou W-J, Liang Z, Shi J-W, Yang H-L, et al. Single-cell transcriptome profiling of the human endometrium of patients with recurrent implantation failure [Internet]. Theranostics. Ivyspring International Publisher; 2022 [cited 2025 Jan 22]. p. 6527–47. Available from: https://doi.org/10.7150/thno.74053

Li J, Xue H, Li T, Chu X, Xin D, Xiong Y, et al. Exosomes derived from mesenchymal stem cells attenuate the progression of atherosclerosis in ApoE−/- mice via miR-let7 mediated infiltration and polarization of M2 macrophage [Internet]. Biochemical and Biophysical Research Communications. Elsevier BV; 2019 [cited 2025 Jan 22]. p. 565–72. Available from: https://doi.org/10.1016/j.bbrc.2019.02.005

Li J, Jiang X, Li H, Gelinsky M, Gu Z. Tailoring Materials for Modulation of Macrophage Fate [Internet]. Advanced Materials. Wiley; 2021a [cited 2025 Jan 22]. Available from: https://doi.org/10.1002/adma.202004172

Li M, Qi L, Li Y, Zhang S, Lin L, Zhou L, et al. Association of Pericardiac Adipose Tissue With Coronary Artery Disease [Internet]. Front. Endocrinol. Frontiers Media SA; 2021b [cited 2025 Jan 22]. Available from: https://doi.org/10.3389/fendo.2021.724859

Li M, Yu J, Guo G, Shen H. Interactions between Macrophages and Biofilm during Staphylococcus aureus-Associated Implant Infection: Difficulties and Solutions [Internet]. J Innate Immun. S. Karger AG; 2023 [cited 2025 Jan 22]. p. 499–515. Available from: https://doi.org/10.1159/000530385

Liang G, Zhu Y, Ali DJ, Tian T, Xu H, Si K, et al. Engineered exosomes for targeted co-delivery of miR-21 inhibitor and chemotherapeutics to reverse drug resistance in colon cancer [Internet]. J Nanobiotechnol. Springer Science and Business Media LLC; 2020 [cited 2025 Jan 22]. Available from: https://doi.org/10.1186/s12951-019-0563-2

Liang H, Wu X, Zhao G, Feng K, Ni K, Sun X. Renal Clearable Ultrasmall Single-Crystal Fe Nanoparticles for Highly Selective and Effective Ferroptosis Therapy and Immunotherapy [Internet]. J. Am. Chem. Soc. American Chemical Society (ACS); 2021 [cited 2025 Jan 22]. p.

15812–23. Available from: https://doi.org/10.1021/jacs.1c07471

Libby P, Theroux P. Pathophysiology of Coronary Artery Disease [Internet]. Circulation. Ovid Technologies (Wolters Kluwer Health); 2005 [cited 2025 Jan 22]. p. 3481–8. Available from: https://doi.org/10.1161/circulationaha.105.537878

Libby P. Inflammation and cardiovascular disease mechanisms [Internet]. The American Journal of Clinical Nutrition. Elsevier BV; 2006 [cited 2025 Jan 22]. p. 456S-460S. Available from: https://doi.org/10.1093/ajcn/83.2.456s

Lin T-F, Chou C-L, Hsieh C-J, Wu Y-J, Chen Y-C, Wu T-W, et al. Association of Common Variants in OLA1 Gene with Preclinical Atherosclerosis [Internet]. IJMS. MDPI AG; 2022 [cited 2025 Jan 22]. p. 11511. Available from: https://doi.org/10.3390/ijms231911511

Liu J, Qiu X, Lv Y, Zheng C, Dong Y, Dou G, et al. Apoptotic bodies derived from mesenchymal stem cells promote cutaneous wound healing via regulating the functions of macrophages [Internet]. Stem Cell Res Ther. Springer Science and Business Media LLC; 2020a [cited 2025 Jan 22]. Available from: https://doi.org/10.1186/s13287-020-02014-w

Liu Y, Liu X, Zhou J, Liang S. MicroRNA-302a promotes neointimal formation following carotid artery injury in mice by targeting PHLPP2 thus increasing Akt signaling [Internet]. Acta Pharmacol Sin. Springer Science and Business Media LLC; 2020b [cited 2025 Jan 22]. p. 550–9. Available from: https://doi.org/10.1038/s41401-020-0440-4

Liu X, Xia S, Zhang Z, Wu H, Lieberman J. Channelling inflammation: gasdermins in physiology and disease [Internet]. Nat Rev Drug Discov. Springer Science and Business Media LLC; 2021 [cited 2025 Jan 22]. p. 384–405. Available from: https://doi.org/10.1038/s41573-021-00154-z

Lovren F, Pan Y, Quan A, Singh KK, Khan R, Gupta N, et al. BRCA1 shields vascular smooth muscle cells from oxidative stress [Internet]. The Journal of Thoracic and Cardiovascular Surgery. Elsevier BV; 2014 [cited 2025 Jan 22]. p. 1946–1955.e1. Available from: https://doi.org/10.1016/j.jtcvs.2013.09.060

Lu D, Chatterjee S, Xiao K, Riedel I, Huang C-K, Costa A, et al. A circular RNA derived from the insulin receptor locus protects against doxorubicin-induced cardiotoxicity [Internet]. European Heart Journal. Oxford University Press (OUP); 2022 [cited 2025 Jan 22]. p. 4496–511. Available from: https://doi.org/10.1093/eurheartj/ehac337

Ma J-D, Jing J, Wang J-W, Yan T, Li Q-H, Mo Y-Q, et al. A novel function of artesunate on inhibiting migration and invasion of fibroblast-like synoviocytes from rheumatoid arthritis patients [Internet]. Arthritis Res Ther. Springer Science and Business Media LLC; 2019a [cited 2025 Jan 22]. Available from:https://doi.org/10.1186/s13075-019-1935-6

Ma L, Hernandez MO, Zhao Y, Mehta M, Tran B, Kelly M, et al. Tumor Cell Biodiversity Drives Microenvironmental Reprogramming in Liver Cancer [Internet]. Cancer Cell. Elsevier BV; 2019b [cited 2025 Jan 22]. p. 418–430.e6. Available from: https://doi.org/10.1016/j.ccell.2019.08.007

Makover ME, Shapiro MD, Toth PP. There is urgent need to treat atherosclerotic cardiovascular disease risk earlier, more intensively, and with greater precision: A review of current practice and recommendations for improved effectiveness [Internet]. American Journal of Preventive Cardiology. Elsevier BV; 2022 [cited 2025 Jan 22]. p. 100371. Available from: https://doi.org/10.1016/j.ajpc.2022.100371

Malakar AKr, Choudhury D, Halder B, Paul P, Uddin A, Chakraborty S. A review on coronary artery disease, its risk factors, and therapeutics [Internet]. Journal Cellular Physiology. Wiley; 2019 [cited 2025 Jan 22]. p. 16812–23. Available from: https://doi.org/10.1002/jcp.28350

Mao X, Xu J, Wang W, Liang C, Hua J, Liu J, et al. Crosstalk between cancer-associated fibroblasts and immune cells in the tumor microenvironment: new findings and future perspectives [Internet]. Mol Cancer. Springer Science and Business Media LLC; 2021 [cited 2025 Jan 22]. Available from: https://doi.org/10.1186/s12943-021-01428-1

Medina-Leyte DJ, Zepeda-García O, Domínguez-Pérez M, González-Garrido A, Villarreal-Molina T, Jacobo-Albavera L. Endothelial Dysfunction, Inflammation and Coronary Artery Disease: Potential Biomarkers and Promising Therapeutical Approaches [Internet]. IJMS. MDPI AG; 2021 [cited 2025 Jan 22]. p. 3850. Available from: https://doi.org/10.3390/ijms22083850

Mehta AK, Cheney EM, Hartl CA, Pantelidou C, Oliwa M, Castrillon JA, et al. Targeting immunosuppressive macrophages overcomes PARP inhibitor resistance in BRCA1-associated triple-negative breast cancer [Internet]. Nat Cancer. Springer Science and Business Media LLC; 2020 [cited 2025 Jan 22]. p. 66–82. Available from: https://doi.org/10.1038/s43018-020-00148-7

Melamed JR, Yerneni SS, Arral ML, LoPresti ST, Chaudhary N, Sehrawat A, et al. Ionizable lipid nanoparticles deliver mRNA to pancreatic β cells via macrophage-mediated gene transfer [Internet]. Sci. Adv. American Association for the Advancement of Science (AAAS); 2023 [cited 2025 Jan 22]. Available from: https://doi.org/10.1126/sciadv.ade1444

Meng H, Ruan J, Yan Z, Chen Y, Liu J, Li X, et al. New Progress in Early Diagnosis of Atherosclerosis [Internet]. IJMS. MDPI AG; 2022 [cited 2025 Jan 22]. p. 8939. Available from: https://doi.org/10.3390/ijms23168939

Mohd Idrus FN, Ahmad NS, Hoe CH, Azlan M, Norfuad FA, Yusof Z, et al. Differential polarization and the expression of efferocytosis receptor MerTK on M1 and M2 macrophages isolated from coronary artery disease patients [Internet]. BMC Immunol. Springer Science and Business Media LLC; 2021 [cited 2025 Jan 22]. Available from: https://doi.org/10.1186/s12865-021-00410-2

Moreau K, Dizin E, Ray H, Luquain C, Lefai E, Foufelle F, et al. BRCA1 Affects Lipid Synthesis through Its Interaction with Acetyl-CoA Carboxylase [Internet]. Journal of Biological Chemistry. Elsevier BV; 2006 [cited 2025 Jan 22]. p. 3172–81. Available from: https://doi.org/10.1074/jbc.m504652200

Mosquera JV, Auguste G, Wong D, Turner AW, Hodonsky CJ, Alvarez-Yela AC, et al. Integrative single-cell meta-analysis reveals disease-relevant vascular cell states and markers in human atherosclerosis [Internet]. Cell Reports. Elsevier BV; 2023 [cited 2025 Jan 22]. p. 113380. Available from: https://doi.org/10.1016/j.celrep.2023.113380

Muskan M, Abeysinghe P, Cecchin R, Branscome H, Morris KV, Kashanchi F. Therapeutic potential of RNA-enriched extracellular vesicles: The next generation in RNA delivery via biogenic nanoparticles [Internet]. Molecular Therapy. Elsevier BV; 2024 [cited 2025 Jan 22]. p. 2939–49. Available from: https://doi.org/10.1016/j.ymthe.2024.02.025

Nakamura K, Miyoshi T, Yoshida M, Akagi S, Saito Y, Ejiri K, et al. Pathophysiology and Treatment of Diabetic Cardiomyopathy and Heart Failure in Patients with Diabetes Mellitus [Internet]. IJMS. MDPI AG; 2022 [cited 2025 Jan 22]. p. 3587. Available from: https://doi.org/10.3390/ijms23073587

Nie C, Zhou XA, Zhou J, Liu Z, Gu Y, Liu W, et al. A transcription-independent mechanism determines rapid periodic fluctuations of BRCA1 expression [Internet]. The EMBO Journal. Springer Science and Business Media LLC; 2023 [cited 2025 Jan 22]. Available from: https://doi.org/10.15252/embj.2022111951

Olsen MB, Gregersen I, Sandanger Ø, Yang K, Sokolova M, Halvorsen BE, et al. Targeting the Inflammasome in Cardiovascular Disease [Internet]. JACC: Basic to Translational Science. Elsevier BV; 2022 [cited 2025 Jan 22]. p. 84–98. Available from: https://doi.org/10.1016/j.jacbts.2021.08.006

Otero-Ortega L, Gómez de Frutos MC, Laso-García F, Rodríguez-Frutos B, Medina-Gutiérrez E, López JA, et al. RETRACTED: Exosomes promote restoration after an experimental animal model of intracerebral hemorrhage [Internet]. J Cereb Blood Flow Metab. SAGE Publications; 2017 [cited 2025 Jan 22]. p. 767–79. Available from: https://doi.org/10.1177/0271678x17708917

Oubaddou Y, Ben Ali F, Oubaqui FE, Qmichou Z, Bakri Y, Ameziane El Hassani R. The Tumor Suppressor BRCA1/2, Cancer Susceptibility and Genome Instability in Gynecological and Mammary Cancers [Internet]. Asian Pac J Cancer Prev. EpiSmart Science Vector Ltd; 2023 [cited 2025 Jan 22]. p. 3139–53. Available from: https://doi.org/10.31557/apjcp.2023.24.9.3139

Pal B, Chen Y, Vaillant F, Capaldo BD, Joyce R, Song X, et al. A single-cell RNA expression atlas of normal, preneoplastic and tumorigenic states in the human breast [Internet]. The EMBO Journal. Springer Science and Business Media LLC; 2021 [cited 2025 Jan 22]. Available from: https://doi.org/10.15252/embj.2020107333

Pan H, Xue C, Auerbach BJ, Fan J, Bashore AC, Cui J, et al. Single-Cell Genomics Reveals a Novel Cell State During Smooth Muscle Cell Phenotypic Switching and Potential Therapeutic Targets for Atherosclerosis in Mouse and Human [Internet]. Circulation. Ovid Technologies (Wolters Kluwer Health); 2020 [cited 2025 Jan 22]. p. 2060–75. Available from: https://doi.org/10.1161/circulationaha.120.048378

Pan Q, Cheng Y, Cheng D. Identification of CD8+ T Cell-Related Genes: Correlations with Immune Phenotypes and Outcomes of Liver Cancer [Internet]. Journal of Immunology Research. Hindawi Limited; 2021 [cited 2025 Jan 22]. p. 1–17. Available from: https://doi.org/10.1155/2021/9960905

Park M-J, Park Y, Choi JW, Baek J-A, Jeong HY, Na HS, et al. Establishment of a humanized animal model of systemic sclerosis in which T helper-17 cells from patients with systemic sclerosis infiltrate and cause fibrosis in the lungs and skin [Internet]. Exp Mol Med. Springer Science and Business Media LLC; 2022 [cited 2025 Jan 22]. p. 1577–85. Available from: https://doi.org/10.1038/s12276-022-00860-7

Piperigkou Z, Tzaferi K, Makrokanis G, Cheli K, Karamanos NK. The microRNA-cell surface proteoglycan axis in cancer progression [Internet]. American Journal of Physiology-Cell Physiology. American Physiological Society; 2022 [cited 2025 Jan 22]. p. C825–32. Available from: https://doi.org/10.1152/ajpcell.00041.2022

Qiao L, Ma J, Zhang Z, Sui W, Zhai C, Xu D, et al. Deficient Chaperone-Mediated Autophagy Promotes Inflammation and Atherosclerosis [Internet]. Circulation Research. Ovid Technologies (Wolters Kluwer Health); 2021 [cited 2025 Jan 22]. p. 1141–57. Available from: https://doi.org/10.1161/circresaha.121.318908

Räber L, Ueki Y, Otsuka T, Losdat S, Häner JD, Lonborg J, et al. Effect of Alirocumab Added to High-Intensity Statin Therapy on Coronary Atherosclerosis in Patients With Acute Myocardial Infarction [Internet]. JAMA. American Medical Association (AMA); 2022 [cited 2025 Jan 22]. p. 1771. Available from: https://doi.org/10.1001/jama.2022.5218

Ragni E, Palombella S, Lopa S, Talò G, Perucca Orfei C, De Luca P, et al. Innovative Visualization and Quantification of Extracellular Vesicles Interaction with and Incorporation in Target Cells in 3D Microenvironments [Internet]. Cells. MDPI AG; 2020 [cited 2025 Jan 22]. p. 1180. Available from: https://doi.org/10.3390/cells9051180

Rangel-Ramírez VV, González-Sánchez HM, Lucio-García C. Exosomes: from biology to immunotherapy in infectious diseases [Internet]. Infectious Diseases. Informa UK Limited; 2022 [cited 2025 Jan 22]. p. 79–107. Available from: https://doi.org/10.1080/23744235.2022.2149852

Ritchie ME, Phipson B, Wu D, Hu Y, Law CW, Shi W, et al. limma powers differential expression analyses for RNA-sequencing and microarray studies [Internet]. Nucleic Acids Research. Oxford University Press (OUP); 2015 [cited 2025 Jan 22]. p. e47–e47. Available from: https://doi.org/10.1093/nar/gkv007

Samstein RM, Krishna C, Ma X, Pei X, Lee K-W, Makarov V, et al. Mutations in BRCA1 and BRCA2 differentially affect the tumor microenvironment and response to checkpoint blockade immunotherapy [Internet]. Nat Cancer. Springer Science and Business Media LLC; 2020 [cited 2025 Jan 22]. p. 1188–203. Available from: https://doi.org/10.1038/s43018-020-00139-8

Sánchez-Lorenzo L, Salas-Benito D, Villamayor J, Patiño-García A, González-Martín A. The BRCA Gene in Epithelial Ovarian Cancer [Internet]. Cancers. MDPI

AG; 2022 [cited 2025 Jan 22]. p. 1235. Available from: https://doi.org/10.3390/cancers14051235

Sheng S, Li J, Hu X, Wang Y. Regulated cell death pathways in cardiomyopathy [Internet]. Acta Pharmacol Sin. Springer Science and Business Media LLC; 2023 [cited 2025 Jan 22]. p. 1521–35. Available from: https://doi.org/10.1038/s41401-023-01068-9

Shu B, Zhang R-Z, Zhou Y-X, He C, Yang X. METTL3-mediated macrophage exosomal NEAT1 contributes to hepatic fibrosis progression through Sp1/TGF-β1/Smad signaling pathway [Internet]. Cell Death Discov. Springer Science and Business Media LLC; 2022 [cited 2025 Jan 22]. Available from: https://doi.org/10.1038/s41420-022-01036-y

Silvestro S, Gugliandolo A, Chiricosta L, Diomede F, Trubiani O, Bramanti P, et al. MicroRNA Profiling of HL-1 Cardiac Cells-Derived Extracellular Vesicles [Internet]. Cells. MDPI AG; 2021 [cited 2025 Jan 22]. p. 273. Available from: https://doi.org/10.3390/cells10020273

Solomon CU, McVey DG, Andreadi C, Gong P, Turner L, Stanczyk PJ, et al. Effects of Coronary Artery Disease–Associated Variants on Vascular Smooth Muscle Cells [Internet]. Circulation. Ovid Technologies (Wolters Kluwer Health); 2022 [cited 2025 Jan 22]. p. 917–29. Available from: https://doi.org/10.1161/circulationaha.121.058389

Takaoka M, Miki Y. BRCA1 gene: function and deficiency [Internet]. Int J Clin Oncol. Springer Science and Business Media LLC; 2017 [cited 2025 Jan 22]. p. 36–44. Available from: https://doi.org/10.1007/s10147-017-1182-2

Takeda H, Dondzillo A, Randall JA, Gubbels SP. Selective ablation of cochlear hair cells promotes engraftment of human embryonic stem cell-derived progenitors in the mouse organ of Corti [Internet]. Stem Cell Res Ther. Springer Science and Business Media LLC; 2021 [cited 2025 Jan 22]. Available from: https://doi.org/10.1186/s13287-021-02403-9

Tan S, Tang H, Wang Y, Xie P, Li H, Zhang Z, et al. Tumor cell-derived exosomes regulate macrophage polarization: Emerging directions in the study of tumor genesis and development [Internet]. Heliyon. Elsevier BV; 2023 [cited 2025 Jan 22]. p. e19296. Available from: https://doi.org/10.1016/j.heliyon.2023.e19296

Thakur A, Johnson A, Jacobs E, Zhang K, Chen J, Wei Z, et al. Energy Sources for Exosome Communication in a Cancer Microenvironment [Internet]. Cancers. MDPI AG; 2022 [cited 2025 Jan 22]. p. 1698. Available from: https://doi.org/10.3390/cancers14071698

Trapnell C, Cacchiarelli D, Grimsby J, Pokharel P, Li S, Morse M, et al. The dynamics and regulators of cell fate decisions are revealed by pseudotemporal ordering of single cells [Internet]. Nat Biotechnol. Springer Science and Business Media LLC; 2014 [cited 2025 Jan 22]. p. 381–6. Available from: https://doi.org/10.1038/nbt.2859

Tutt ANJ, Garber JE, Kaufman B, Viale G, Fumagalli D, Rastogi P, et al. Adjuvant Olaparib for Patients with BRCA1- or BRCA2-Mutated Breast Cancer [Internet]. N Engl J Med. Massachusetts Medical Society; 2021 [cited 2025 Jan 22]. p. 2394–405. Available from: https://doi.org/10.1056/nejmoa2105215

Vázquez-García I, Uhlitz F, Ceglia N, Lim JLP, Wu M, Mohibullah N, et al. Ovarian cancer mutational processes drive site-specific immune evasion [Internet]. Nature. Springer Science and Business Media LLC; 2022 [cited 2025 Jan 22]. p. 778–86. Available from: https://doi.org/10.1038/s41586-022-05496-1

Velusamy R, Nolan M, Murphy A, Thavendiranathan P, Marwick TH. Screening for Coronary Artery Disease in Cancer Survivors [Internet]. JACC: CardioOncology. Elsevier BV; 2023 [cited 2025 Jan 22]. p. 22–38. Available from: https://doi.org/10.1016/j.jaccao.2022.12.007

Wang Z, Zhu H, Shi H, Zhao H, Gao R, Weng X, et al. Exosomes derived from M1 macrophages aggravate neointimal hyperplasia following carotid artery injuries in mice through miR-222/CDKN1B/CDKN1C pathway [Internet]. Cell Death Dis. Springer Science and Business Media LLC; 2019 [cited 2025 Jan 22]. Available from: https://doi.org/10.1038/s41419-019-1667-1

Wang C, Wang L, Guan X, Yue C. MiR-4303 relieves chondrocyte inflammation by targeting ASPN in osteoarthritis [Internet]. J Orthop Surg Res. Springer Science and Business Media LLC; 2021a [cited 2025 Jan 22]. Available from: https://doi.org/10.1186/s13018-021-02731-9

Wang Y, Zhang L, Wu G-R, Zhou Q, Yue H, Rao L-Z, et al. MBD2 serves as a viable target against pulmonary fibrosis by inhibiting macrophage M2 program [Internet]. Sci. Adv. American Association for the Advancement of Science (AAAS); 2021b [cited 2025 Jan 22]. Available from: https://doi.org/10.1126/sciadv.abb6075

Wei Y, Lan B, Zheng T, Yang L, Zhang X, Cheng L, et al. GSDME-mediated pyroptosis promotes the progression and associated inflammation of atherosclerosis [Internet]. Nat Commun. Springer Science and Business Media LLC; 2023 [cited 2025 Jan 22]. Available from: https://doi.org/10.1038/s41467-023-36614-w

Wu H, Zheng J, Xu S, Fang Y, Wu Y, Zeng J, et al. Mer regulates microglial/macrophage M1/M2 polarization and alleviates neuroinflammation following traumatic brain injury [Internet]. J Neuroinflammation. Springer Science and Business Media LLC; 2021a [cited 2025 Jan 22]. Available from: https://doi.org/10.1186/s12974-020-02041-7

Wu M-M, Wang Q-M, Huang B-Y, Mai C-T, Wang C-L, Wang T-T, et al. Dioscin ameliorates murine ulcerative colitis by regulating macrophage polarization [Internet]. Pharmacological Research. Elsevier BV; 2021b [cited 2025 Jan 22]. p. 105796. Available from: https://doi.org/10.1016/j.phrs.2021.105796

Wu T, Liu Y, Cao Y, Liu Z. Engineering Macrophage Exosome Disguised Biodegradable Nanoplatform for Enhanced Sonodynamic Therapy of Glioblastoma [Internet]. Advanced Materials. Wiley; 2022a [cited 2025 Jan 22]. Available from: https://doi.org/10.1002/adma.202110364

Wu X, Qin K, Iroegbu CD, Xiang K, Peng J, Guo J, et al. Genetic analysis of potential biomarkers and therapeutic targets in ferroptosis from coronary artery disease [Internet]. J Cellular Molecular Medi. Wiley; 2022b [cited 2025 Jan 22]. p. 2177–90. Available from: https://doi.org/10.1111/jcmm.17239

Xiang Q, Yi X, Zhu X-H, Wei X, Jiang D-S. Regulated cell death in myocardial ischemia–reperfusion injury

[Internet]. Trends in Endocrinology & Metabolism. Elsevier BV; 2024 [cited 2025 Jan 22]. p. 219–34. Available from: https://doi.org/10.1016/j.tem.2023.10.010

Xiao H, Zhang M, Wu H, Wu J, Hu X, Pei X, et al. CIRKIL Exacerbates Cardiac Ischemia/Reperfusion Injury by Interacting With Ku70 [Internet]. Circulation Research. Ovid Technologies (Wolters Kluwer Health); 2022 [cited 2025 Jan 22]. Available from: https://doi.org/10.1161/circresaha.121.318992

Xie B, Lu C, Chen C, Zhou J, Deng Z. miR-135a Alleviates Silica-Induced Pulmonary Fibrosis by Targeting NF-κB/Inflammatory Signaling Pathway [Internet]. Mediators of Inflammation. Hindawi Limited; 2020 [cited 2025 Jan 22]. p. 1–13. Available from: https://doi.org/10.1155/2020/1231243

Yalcinkaya M, Liu W, Thomas L-A, Olszewska M, Xiao T, Abramowicz S, et al. BRCC3-Mediated NLRP3 Deubiquitylation Promotes Inflammasome Activation and Atherosclerosis in Tet2 Clonal Hematopoiesis [Internet]. Circulation. Ovid Technologies (Wolters Kluwer Health); 2023 [cited 2025 Jan 22]. p. 1764–77. Available from: https://doi.org/10.1161/circulationaha.123.065344

Yan W, Li T, Yin T, Hou Z, Qu K, Wang N, et al. M2 macrophage-derived exosomes promote the c-KIT phenotype of vascular smooth muscle cells during vascular tissue repair after intravascular stent implantation [Internet]. Theranostics. Ivyspring International Publisher; 2020 [cited 2025 Jan 22]. p. 10712–28. Available from: https://doi.org/10.7150/thno.46143

Yang Z, Zhang Y, Yang S, Ding Y, Qu Y. Low-Dose Resveratrol Inhibits RIPK3-Mediated Necroptosis and Delays the Onset of Age-Related Hearing Loss [Internet]. Front. Pharmacol. Frontiers Media SA; 2022 [cited 2025 Jan 22]. Available from: https://doi.org/10.3389/fphar.2022.910308

Yang P, Luo Q, Wang X, Fang Q, Fu Z, Li J, et al. Comprehensive Analysis of Fibroblast Activation Protein Expression in Interstitial Lung Diseases [Internet]. Am J Respir Crit Care Med. American Thoracic Society; 2023 [cited 2025 Jan 22]. p. 160–72. Available from: https://doi.org/10.1164/rccm.202110-2414oc

Yang Y, Huang K, Jiang H, Wang S, Xu X, Liu Y, et al. Unveiling the role of circRBBP7 in myoblast proliferation and differentiation: A novel regulator of muscle development [Internet]. The FASEB Journal. Wiley; 2024 [cited 2025 Jan 22]. Available from: https://doi.org/10.1096/fj.202302599rr

Yap J, Irei J, Lozano-Gerona J, Vanapruks S, Bishop T, Boisvert WA. Macrophages in cardiac remodelling after myocardial infarction [Internet]. Nat Rev Cardiol. Springer Science and Business Media LLC; 2023 [cited 2025 Jan 22]. p. 373–85. Available from: https://doi.org/10.1038/s41569-022-00823-5

Yarden RI, Brody LC. BRCA1 interacts with components of the histone deacetylase complex [Internet]. Proc. Natl. Acad. Sci. U.S.A. Proceedings of the National Academy of Sciences; 1999 [cited 2025 Jan 22]. p. 4983–8. Available from: https://doi.org/10.1073/pnas.96.9.4983

Yekhtin Z, Khuja I, Meiri D, Or R, Almogi-Hazan O. Differential Effects of D9 Tetrahydrocannabinol (THC)- and Cannabidiol (CBD)-Based Cannabinoid Treatments on Macrophage Immune Function In Vitro and on Gastrointestinal Inflammation in a Murine Model [Internet]. Biomedicines. MDPI AG; 2022 [cited 2025 Jan 22]. p. 1793. Available from: https://doi.org/10.3390/biomedicines10081793

Yin H, Zhang X, Yang P, Zhang X, Peng Y, Li D, et al. RNA m6A methylation orchestrates cancer growth and metastasis via macrophage reprogramming [Internet]. Nat Commun. Springer Science and Business Media LLC; 2021 [cited 2025 Jan 22]. Available from: https://doi.org/10.1038/s41467-021-21514-8

Yuhas SC, Mishra A, DeWeese TL, Greenberg MM. Suppression of DNA Polymerase β Activity Is Synthetically Lethal in BRCA1-Deficient Cells [Internet]. ACS Chem. Biol. American Chemical Society (ACS); 2021 [cited 2025 Jan 22]. p. 1339–43. Available from: https://doi.org/10.1021/acschembio.1c00385

Yun TJ, Igarashi S, Zhao H, Perez OA, Pereira MR, Zorn E, et al. Human plasmacytoid dendritic cells mount a distinct antiviral response to virus-infected cells [Internet]. Sci. Immunol. American Association for the Advancement of Science (AAAS); 2021 [cited 2025 Jan 22]. Available from: https://doi.org/10.1126/sciimmunol.abc7302

Zhai M, Gong S, Luan P, Shi Y, Kou W, Zeng Y, et al. Extracellular traps from activated vascular smooth muscle cells drive the progression of atherosclerosis [Internet]. Nat Commun. Springer Science and Business Media LLC; 2022 [cited 2025 Jan 22]. Available from: https://doi.org/10.1038/s41467-022-35330-1

Zhang Q-F, Li J, Jiang K, Wang R, Ge J, Yang H, et al. CDK4/6 inhibition promotes immune infiltration in ovarian cancer and synergizes with PD-1 blockade in a B cell-dependent manner [Internet]. Theranostics. Ivyspring International Publisher; 2020 [cited 2025 Jan 22]. p. 10619–33. Available from: https://doi.org/10.7150/thno.44871

Zhang M, Gao J, Zhao X, Zhao M, Ma D, Zhang X, et al. p38α in macrophages aggravates arterial endothelium injury by releasing IL-6 through phosphorylating megakaryocytic leukemia 1 [Internet]. Redox Biology. Elsevier BV; 2021 [cited 2025 Jan 22]. p. 101775. Available from: https://doi.org/10.1016/j.redox.2020.101775

Zhang Z, Xu Y, Cao C, Wang B, Guo J, Qin Z, et al. Exosomes as a messager to regulate the crosstalk between macrophages and cardiomyocytes under hypoxia conditions [Internet]. J Cellular Molecular Medi. Wiley; 2022 [cited 2025 Jan 22]. p. 1486–500. Available from: https://doi.org/10.1111/jcmm.17162

Zhi L, Zhao L, Zhang X, Liu W, Gao B, Wang F, et al. SLCO1B3 promotes colorectal cancer tumorigenesis and metastasis through STAT3 [Internet]. Aging. Impact Journals, LLC; 2021 [cited 2025 Jan 22]. p. 22164–75. Available from: https://doi.org/10.18632/aging.203502

Publisher's Note Springer Nature remains neutral with regard to jurisdictional claims in published maps and institutional affiliations.